A DIRECT METHOD FOR SOLVING AN ANISOTROPIC MEAN CURVATURE FLOW OF PLANE CURVES WITH AN EXTERNAL FORCE

KAROL MIKULA * AND DANIEL ŠEVČOVIČ †

Abstract. A new method for solution of the evolution of plane curves satisfying the geometric equation $v = \beta(x, k, \nu)$ where v is the normal velocity, k and ν are the curvature and tangential angle of a plane curve $\Gamma \subset \mathbb{R}^2$ at the point $x \in \Gamma$ is proposed. We derive a governing system of partial differential equations for the curvature, tangential angle, local length and position vector of an evolving family of plane curves and prove local in time existence of a classical solution. These equations include a nontrivial tangential velocity functional governing a uniform redistribution of grid points and thus preventing numerically computed solutions from forming various instabilities. We discretize the governing system of equations in order to find a numerical solution for 2D anisotropic interface motions with applications in thermomechanics and medical image segmentation problems.

1. Introduction. In this paper we study evolution of a closed smooth embedded plane curve $\Gamma : S^1 \to \mathbb{R}^2$. The normal velocity v of an evolving family of plane curves $\Gamma_t, t \geq 0$, is assumed to be a function of the curvature k, tangential angle ν and position vector $x \in \Gamma_t$,

$$v = \beta(x, k, \nu)\,. \tag{1.1}$$

Geometric equations of the form (1.1) appear within a large variety of applied problems. They can be often found in the material science, dynamics of phase boundaries in thermomechanics, in modeling of flame front propagation, in combustion, in computations of first arrival times of seismic waves, in computational geometry, robotics, semiconductors industry, etc. They also have a special importance in image processing and computer vision. A particular choice $v = \beta(k)$ leads to the so-called morphological image and shape multiscale analysis studied by Alvarez, Guichard, Lions and Morel [2]. An image silhouette corresponding to a level line Γ of the image intensity function is driven by Eq. (1.1). Sapiro and Tannenbaum in [36] considered a special choice of the normal velocity $\beta(k) = k^{1/3}$ for the affine invariant analysis of shapes. A typical case in which the normal velocity v may depend on the position vector x can be found in image segmentation. Two of applications which we are mainly interested in will be described in more details in next sections. For a comprehensive overview of other important applications of the geometric Eq. (1.1) we refer to a recent book by Sethian [39].

We follow the so-called direct approach for solving the geometric Eq. (1.1). In comparison to the other well-known techniques, like e.g. level-set method ([33], [39]) or phase-field approximations (see [10], [34], [9]), in the direct approach one space dimensional evolutionary problems are solved. A first idea behind the direct approach consists of representation of a family of embedded curves Γ_t by the position vector $x \in \mathbb{R}^2$, i.e. $\Gamma_t = \text{Image}(x(.,t))$ where x is a solution to the geometric equation

$$\partial_t x = \beta \vec{N} + \alpha \vec{T} \tag{1.2}$$

where $\beta = \beta(x, k, \nu)$, $\vec{N} = (-\sin\nu, \cos\nu)$ and $\vec{T} = (\cos\nu, \sin\nu)$ are the unit inward normal and tangent vectors, respectively. For the normal velocity $v = \partial_t x.\vec{N}$ we have $v = \beta(x, k, \nu)$.

* Department of Mathematics, Slovak University of Technology, Radlinského 11, 813 68 Bratislava, Slovak Republic (mikula@vox.svf.stuba.sk).

† Inst. of Applied Mathematics, Faculty of Mathematics, Physics & Informatics, Comenius University, 842 48 Bratislava, Slovak Republic (sevcovic@fmph.uniba.sk).

This work was supported by grants No. 1/7132/20, No. 1/7677/20 of the Slovak Scientific Grant Agency VEGA and by the German Sonderforschungsbereich 359: Reactive Flows, Diffusion and Transport. The first author would like to thank Professor Willi Jäger for invitation to IWR, University of Heidelberg, where a substantial part of this work has been completed.

Notice that the presence of a tangential velocity functional α has no impact on the shape of evolving curves and therefore a "natural" setting $\alpha = 0$ has been chosen for analytical as well as numerical treatment in the literature ([1], [19], [20], [6], [17], [18]). An important role of a nontrivial tangential term has been discovered and utilized in ([21], [27], [16], [22], [31], [32]). In [32], Eq. (1.1) has been solved with $\beta = \beta(k, \nu)$ nonlinearly depending on the curvature k. The tangential term α appearing in (1.2) has been chosen in such a way that an initial distribution of grid points representing a curve is preserved during evolution. In case of isotropic and linear dependence of the flow on curvature, the same redistribution strategy has been suggested by Hou *et al.* in [21], [22]. Such approach significantly improved and stabilized all computations realized by the direct method which has been documented by a variety of numerical experiments in [21], [22], [32].

Here we present a direct method for solving the geometric Eq. (1.1) with the normal velocity v involving a curvature, anisotropy, spatial position dependence and strong external force. Our idea is to investigate scalar (i.e. one space dimensional) parabolic equations for various geometric quantities like e.g. a curvature equation. In the case of a convex initial curve such an approach was discussed in [29], [30] where the so-called curve shortening equation has been solved in a fixed spatial interval determined by a range of values of the tangential angle. In the nonconvex case the situation is more difficult because the tangential angle cannot be used as a fixed domain parametrization. However, as it will be shown in this paper for general situation (1.1), a closed system of equations for both geometrical quantities k and ν can be derived enabling us to handle evolution of nonconvex curves also. Particular cases of such equations have been considered in [21], [22] for linear curvature driven motions and in [32] for anisotropic nonlinear curvature flows without spatial dependence of the evolution.

In this paper we generalize the direct approaches studied in [21], [29], [22], [32]. We derive a closed evolutionary system of parabolic and ordinary differential equations in one space dimension governing the evolution of plane curves satisfying (1.1). The system contains intrinsic parabolic equations for the curvature, tangential angle and ordinary differential equations for evolution of the local length element and position vector. The governing system of equations includes a nontrivial tangential velocity functional α which in comparison to [21], [22], [32] force a curve representation to be uniform without any condition to its initial grid points distribution. By this approach, after numerical discretization, we can handle complicated curve dynamics driven by curvature, anisotropy, constant driving force or general velocity vector field applied to the curve. Taking into account a suitable tangential velocity we can prevent numerical solutions from forming numerical instabilities like e.g. merging of grid points or formation of "swallow tails". We can furthermore resolve the so-called sharp corners formation and their evolution. From analytical perspective, we prove short time existence of solution to the general curve evolution model (1.1) and derive further properties like, e.g., Lyapunov functionals.

The governing intrinsic equations are of convection–reaction–diffusion type. Our fully discrete numerical scheme is semi-implicit in time, i.e. all nonlinearities are treated from the previous time step and linear terms are discretized at the current time level. We solve tridiagonal systems in every time step in a fast and simple way. An undesirable, from a numerical point of view, behavior of strong reaction terms is overcome by an appropriate choice of a tangential redistribution functional. We show that stability constraint for our semi-implicit scheme is related to an integral average of $k\beta$ along the curve. Thus the method allows the choosing of larger time steps without loss of stability. Stabilization in the convective terms is obtained by taking a sufficiently fine curve representation.

The outline of the paper is as follows. In the next section we discuss in some detail two applications in which a geometric equation of the form (1.1) naturally occurs. In section 3 we present a governing system of PDEs capable of describing the evolution of plane curves satisfying (1.1). We prove local in time existence of classical solutions by means of the abstract theory of fully nonlinear parabolic equations. Section 4 is devoted to the study of qualitative properties of solutions. We derive several Lyapunov functionals decreasing along trajectories. Section 5 is focused on the problem how to choose a suitable tangential velocity functional α. In section 6 numerical schemes for full space time discretization of the governing system of equations are presented. In the context of the isotropic and anisotropic curve evolution and image segmentation results of numerical simulations are discussed in a detail.

2. Motivation. Throughout the paper we will be mainly concerned with applications in which the normal velocity v may depend on the position vector x, the tangential angle ν and the dependence on the curvature k is linear, i.e. $v = \beta(x, k, \nu)$ where

$$\beta(x, k, \nu) = \delta(x, \nu)\, k + c(x, \nu) \tag{2.1}$$

and $\delta > 0$ and c are smooth coefficients depending on x and ν.

2.1. Interface dynamics. If a solid occupies a subset $\Omega_s(t) \subset \Omega$ and liquid a subset $\Omega_l(t) \subset \Omega$, $\Omega \subset \mathbb{R}^2$, at a time t, then the phase interface is a set $\Gamma_t = \partial\Omega_s(t) \cap \partial\Omega_l(t)$ which is assumed to be a closed smooth embedded curve. The sharp-interface description of the solidification process is then described by the Stefan problem with a surface tension

$$\rho c \partial_t U = \lambda \Delta U \qquad \text{in } \Omega_s(t) \text{ and } \Omega_l(t), \tag{2.2}$$

$$[\lambda \partial_n U]_s^l = -Lv \qquad \text{on } \Gamma_t, \tag{2.3}$$

$$\frac{\delta e}{\sigma}(U - U^*) = -\gamma_2(\nu)k + \gamma_1(\nu)v \text{ on } \Gamma_t, \tag{2.4}$$

accompanied with initial and boundary conditions for the temperature field U and initial position of the interface Γ (see e.g. [38], [9]). The constants ρ, c, λ represent material characteristics (density, specific heat and thermal conductivity), L is latent heat per unit volume, U^* is a melting point and v is normal velocity of the interface. Discontinuity in the heat flux on the interface Γ_t is described by the Stefan condition (2.3). The relationship (2.4) is referred to as the Gibbs–Thomson law on the interface Γ_t, where δe is difference in entropy per unit volume between liquid and solid phases, σ is a constant surface tension, γ_1 is a coefficient of attachment kinetics and dimensionless function γ_2 describes anisotropy of the interface. One can see that the Gibbs–Thomson condition can be viewed as a relationship of the form (2.1). In the series of papers [6, 7, 8], Angenent and Gurtin studied perfect conductors where the problem can be reduced to a single equation on the interface. Following this approach and assuming a constant kinetic coefficient one obtains the equation

$$v = \gamma(\nu)k + F, \tag{2.5}$$

describing the interface dynamics. It is often referred to as the *anisotropic curve shortening equation* with a constant driving force F (energy difference between bulk phases) and a given anisotropy function γ.

2.2. Image segmentation. In the context of image segmentation, detection of object boundaries in an image plays an important role. Suppose an image is represented by a given intensity function $u_0 : R^2 \to [0, 1]$. The problem is to detect edges of the image, i.e. plane curves on which the gradient ∇u_0 is large and thus forming boundaries of a segmented object. The idea is to construct an evolving family of plane curves converging to an edge (see [24]).

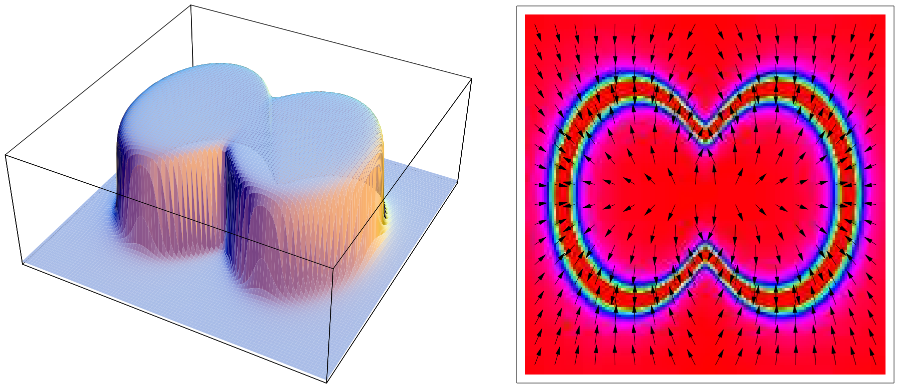

FIG. 2.1. *The image intensity function u_0 (left). The density plot of the function ϕ and corresponding vector field $\vec{W}$ (right).*

One can construct such a family respecting the geometric Eq. (2.1) where $c = c(x, \nu)$ is a driving force and $\delta = \delta(x, \nu) > 0$ is a smoothing coefficient. These functions may depend on the position vector x as well as orientation angle ν of a curve. It is worth noting that if $c > 0$ then the effect of the driving force is to shrink a curve $\Gamma = \Gamma_t$ whereas it tends to expand such curve in the opposite case $c < 0$. In the last decade, edge detection methods based on such a curve evolution approaches were first discussed in [11] and [28] in the level set formulation. Later on, they have been revisited and improved by [12], [13], [14], [25], [26]. In our numerical experiments we will use a generalization of a model proposed by Casseles et al. in [13] and by Kichenassamy et al. in [26]. To this end, let us take a smooth edge detector function $h : [0, \infty) \to (0, \infty)$ such that $h' < 0, h(0) = 1, h(+\infty) = 0$ and $h'(s) \le Ch(s), |h''(s)| \le C, s > 0$, for some constant $C > 0$. A typical example of such a detector function is $h(s) = e^{-\lambda s}$ or $h(s) = 1/(1 + \lambda s^2)$ where $\lambda > 0$ is a parameter (cf. [35]). If the intensity function u_0 is C^2 smooth then the vector field $\vec{W}$ given by

$$\vec{W}(x) = -\nabla \phi(x), \qquad \phi(x) = h(|\nabla u_0(x)|) \tag{2.6}$$

has an important geometric property because it points towards regions where the norm of the gradient ∇u_0 is large (see Fig. 2.1 right). Notice that a possible lack of smoothness of u_0 (e.g. due to a noise) can be overcome by convolving u_0 by a smooth mollifier G_σ having a compact support of a small radius $\sigma > 0$ or by applying a selectively smoothing nonlinear filter ([15], [23]).

Taking into account the geometric property of the vector field $\vec{W}(x)$ we are in a position to define a driving force $c(x, \nu)$ as follows:

$$c(x, \nu) = b(\phi(x))\, \vec{W}(x).\vec{N} = -b(\phi(x))\, \nabla \phi(x).\vec{N} \tag{2.7}$$

where $b = b(\phi)$ and the unit inward normal vector $\vec{N}$ is given by $\vec{N} = (-\sin \nu, \cos \nu)$. Finally, we discuss a suitable choice of a smoothing function $\delta = \delta(x)$. Suppose a curve Γ_t is close to an edge having a large variation in the curvature. In such a case the curvature term in (2.1) works against the forcing term $c(x, \nu)$ driving the motion towards this edge. It may eventually stop the evolution away from the vicinity of an edge. The idea of how to overcome this problem is to construct a function $\delta(x)$ by taking into account the geometric property of the gradient $|\nabla u_0(x)|$ of the image function. Clearly, if a curve Γ is close to an edge then

$|\nabla u_0(x)|$ is large and consequently $\phi(x) = h(|\nabla u_0(x)|)$ is small. This observation leads us to the following choice of a function δ:

$$\delta(x) = a(\phi(x)) \tag{2.8}$$

where $a(\phi)$ is a smooth function, $a(0) = 0$, $a(\phi) > 0$ for $\phi > 0$. As a typical example one can take $\delta(x) = \varepsilon\phi(x)$, i.e. $a(\phi) = \varepsilon\phi$ where $\varepsilon > 0$ is a parameter. In the case $\varepsilon = 1$ and $b(\phi) = 1$ we obtain a model proposed and investigated in [13] and [26].

3. Analysis of the governing equations. In this section we derive a closed system of PDEs governing the evolution of the flow of plane curves satisfying the geometric Eq. (1.1). An embedded regular plane curve Γ will be parameterized by a smooth function $x : S^1 \to \mathbb{R}^2$ such that $\Gamma = \text{Image}(x) = \{x(u), u \in [0,1]\}$ and $|\partial_u x| > 0$. Hereafter, we identify the unit circle S^1 with the interval $[0,1] \approx \mathbb{R}/\mathbb{Z}$ respecting the periodic boundary conditions at $u = 0, 1$. Let s denote the unit arc-length parameterization of a curve $\Gamma = \text{Image}(x)$. Then $ds = |\partial_u x| du$ and the tangent vector $\vec{T}$ and the signed curvature k of Γ satisfy

$$\vec{T} = \partial_s x = |\partial_u x|^{-1}\partial_u x, \qquad k = \partial_s x \wedge \partial_s^2 x = |\partial_u x|^{-3}\partial_u x \wedge \partial_u^2 x\,. \tag{3.1}$$

The unit inward normal vector $\vec{N}$ is chosen in such a way that $\vec{T} \wedge \vec{N} = 1$ where $\vec{a} \wedge \vec{b}$ is the determinant of the 2×2 matrix with column vectors $\vec{a}, \vec{b}$. By ν we denote the tangent angle to Γ, i.e. $\nu = \arg(\vec{T})$. Then $(\cos\nu, \sin\nu) = \vec{T}$. By Frenét's formulae $\partial_s \vec{T} = k\vec{N}$ and $\partial_s \vec{N} = -k\vec{T}$.

Let a regular smooth initial curve $\Gamma_0 = \text{Image}(x_0)$ be given. As it was already sketched in section 1, a flow of plane curves $\Gamma_t = \text{Image}(x(.,t)), \quad t \in [0,T)$, satisfying (1.1) can be represented by a solution $x = x(u,t)$ to the position vector Eq. (1.2). Unfortunately, this equation can not be solved directly because it contains the curvature k depending on higher order derivatives of a solution x itself (see (3.1)). This is why we have to construct a closed system of governing equations for the curvature k, the tangent angle ν, the local length element $g = |\partial_u x|$ and the position vector x. The equations to follow are straightforward modifications of well-known geometric equations derived for the case of zero tangential velocity α (see e.g. [19, 1, 3, 4]). In the case $\alpha \neq 0$ these equations have been derived by the authors in [32]. Recall that the equation for the tangential angle is: $\partial_t \nu = \partial_s \beta + \alpha k$. Since $\partial_s \nu = k$ and $\partial_s \beta = \beta'_k \partial_s k + \beta'_\nu k + \nabla_x \beta.\vec{T}$ we end up with the following closed system of parabolic-ordinary differential equations:

$$\partial_t k = \partial_s^2 \beta + \alpha \partial_s k + k^2 \beta\,, \tag{3.2}$$

$$\partial_t \nu = \beta'_k \partial_s^2 \nu + (\alpha + \beta'_\nu)\partial_s \nu + \nabla_x \beta.\vec{T}\,, \tag{3.3}$$

$$\partial_t g = -gk\beta + \partial_u \alpha\,, \tag{3.4}$$

$$\partial_t x = \beta\vec{N} + \alpha\vec{T}\,, \tag{3.5}$$

where $(u,t) \in [0,1] \times (0,T)$, $ds = g\,du$ and $\vec{T} = \partial_s x = (\cos\nu, \sin\nu)$, $\vec{N} = \vec{T}^\perp = (-\sin\nu, \cos\nu)$. The functional α may depend on the variables k, ν, g, x. A solution (k, ν, g, x) to (3.2) – (3.5) is subject to initial conditions

$$k(.,0) = k_0\,, \quad \nu(.,0) = \nu_0\,, \quad g(.,0) = g_0\,, \quad x(.,0) = x_0(.)\,,$$

and periodic boundary conditions at $u = 0, 1$. Notice that the initial conditions for k_0, ν_0, g_0 and x_0 (the curvature, tangent angle, local length element and position vector of the initial curve Γ_0) must satisfy the following compatibility constraints:

$$g_0 = |\partial_u x_0| > 0\,, \quad k_0 = g_0^{-3}\partial_u x_0 \wedge \partial_u^2 x_0\,, \quad \partial_u \nu_0 = g_0 k_0\,.$$

In the rest of this section we will prove local in time existence of a classical solution of the governing system of Eqs. (3.2) – (3.5) by following the abstract theory of nonlinear analytic semiflows due to Angenent (cf. [5]). If we denote $\Phi = (k, \nu, g, x)$ then the system of governing Eqs. (3.2) – (3.5) can be rewritten as a fully nonlinear PDE of the form

$$\partial_t \Phi = f(\Phi), \qquad \Phi(0) = \Phi_0 \,, \tag{3.6}$$

where $f(\Phi) = F(\Phi, \alpha(\Phi))$ and $F(\Phi, \alpha)$ is the right hand side of (3.2) – (3.5). Let $0 < \varrho < 1$ be fixed. By E_k we denote the following scale of Banach space

$$E_k = c^{2k+\varrho}(S^1) \times c^{2k+\varrho}(S^1) \times c^{1+\varrho}(S^1) \times (c^{2+\varrho}(S^1))^2 \tag{3.7}$$

where $k = 0, \frac{1}{2}, 1$, and $c^{2k+\varrho}(S^1)$ is the "little" Hölder space, i.e. the closure of $C^\infty(S^1)$ in the topology of the Hölder space $C^{2k+\varrho}(S^1)$ (see [3]). If we assume

$$\alpha \in C^1(\mathcal{O}_{\frac{1}{2}}, c^{2+\varrho}(S^1)) \tag{3.8}$$

for any bounded open subset $\mathcal{O}_{\frac{1}{2}} \subset E_{\frac{1}{2}}$ such that $g > 0$ for any $(k, \nu, g, x) \in \mathcal{O}_{\frac{1}{2}}$ and the function $\beta : \mathbb{R}^2 \times \mathbb{R} \times \mathbb{R} \to \mathbb{R}$ is C^4 smooth then the mapping f is C^1 smooth from the open subset $\mathcal{O}_1 = \mathcal{O}_{\frac{1}{2}} \cap E_1 \subset E_1$ into E_0.

If the Fréchet derivative $df(\bar\Phi) \in \mathcal{L}(E_1, E_0)$ belongs to the maximal regularity class $\mathcal{M}_1(E_0, E_1)$ for any $\bar\Phi \in \mathcal{O}_1$ where $\mathcal{O}_1$ is a neighborhood of the initial condition Φ_0 then, by [5, Theorem 2.7], the abstract Eq. (3.6) has a unique solution $\Phi \in Y^{(T)} = C([0,T], E_1) \cap C^1([0,T], E_0)$ on some small enough time interval $[0,T]$. Recall that the class $\mathcal{M}_1(E_0, E_1) \subset \mathcal{L}(E_1, E_0)$ consists of those generators of analytic semigroups $A : D(A) = E_1 \subset E_0 \to E_0$ for which the linear equation $\partial_t \Phi = A\Phi + h(t)$, $0 < t \le 1$, $\Phi(0) = \Phi_0$, has a unique solution $\Phi \in Y^{(1)}$ for any $h \in C([0,1], E_0)$ and $\Phi_0 \in E_1$. In other words, (E_0, E_1) is a maximal parabolic regularity pair.

THEOREM 3.1. *Assume $\Phi_0 = (k_0, \nu_0, g_0, x_0) \in E_1$ where k_0 is the curvature, ν_0 is the tangential vector and $g_0 = |\partial_u x_0| > 0$ is the local length element of an initial regular curve $\Gamma_0 = \mathrm{Image}(x_0)$. If $\beta = \beta(x, k, \nu)$ is a C^4 smooth function such that $\min_{\Gamma_0} \beta'_k(x_0, k_0, \nu_0) > 0$ and α satisfies (3.8) then there exists a unique classical solution $\Phi = (k, \nu, g, x) \in C([0,T], E_1) \cap C^1([0,T], E_0)$ of the governing system of Eqs. (3.2) – (3.5) defined on some small time interval $[0,T]$, $T > 0$. Moreover, if Φ is the maximal solution defined on $[0, T_{max})$ then either $T_{max} = +\infty$ or $\liminf_{t \to T_{max}^-} \min_{\Gamma_t} \beta'_k(x, k, \nu) = 0$ or $T_{max} < +\infty$ and $\max_{\Gamma_t} |k| \to \infty$ as $t \to T_{max}$.*

Proof. Since $\partial_s \nu = k$ and $\partial_s \beta = \beta'_k \partial_s k + \beta'_\nu k + \nabla_x \beta . \vec{T}$ the curvature equation (3.2) can be rewritten in the divergent form

$$\partial_t k = \partial_s(\beta'_k \partial_s k) + \partial_s(\beta'_\nu k) + k \nabla_x \beta . \vec{N} + \partial_s(\nabla_x \beta . \vec{T}) + \alpha \partial_s k + k^2 \beta \,.$$

Let us take an open bounded subset $\mathcal{O}_{\frac{1}{2}} \subset E_{\frac{1}{2}}$ such that $\Phi_0 \in \mathcal{O}_1 = \mathcal{O}_{\frac{1}{2}} \cap E_1 \subset E_1$, $g > 0$, and $\beta'_k(x, k, \nu) > 0$ for any $(k, \nu, g, x) \in \mathcal{O}_1$. The linearization of f at a point $\bar\Phi = (\bar k, \bar\nu, \bar g, \bar x) \in \mathcal{O}_1$ has the form $df(\bar\Phi) = d_\Phi F(\bar\Phi, \bar\alpha) + d_\alpha F(\bar\Phi, \bar\alpha)\, d_\Phi \alpha(\bar\Phi)$ where $\bar\alpha = \alpha(\bar\Phi)$ and

$$d_\Phi F(\bar\Phi, \bar\alpha) = \partial_u \bar D \partial_u + \bar B \partial_u + \bar C \,, \quad d_\alpha F(\bar\Phi, \bar\alpha) = \left(\bar g^{-1} \partial_u \bar k \,,\ \bar k \,,\ \partial_u \,,\ \bar{\vec{T}} \right)$$

$\bar D = \mathrm{diag}(\bar D_{11}, \bar D_{22}, 0, 0, 0)$, $\bar D_{11} = \bar D_{22} = \bar g^{-2} \beta'_k(\bar x, \bar k, \bar\nu) \in C^{1+\varrho}(S^1)$ and $\bar B, \bar C$ are 5×5 matrices with $C^\varrho(S^1)$ smooth coefficients. Moreover, $\bar B_{ij} = 0$ for $i = 3, 4, 5$ and

$\bar{C}_{3j} \in C^{1+\varrho}$, $\bar{C}_{ij} \in C^{2+\varrho}$ for $i = 4, 5$ and all j. The linear operator A_1 defined by $A_1\Phi = \partial_u(\bar{D}\partial_u\Phi)$, $D(A_1) = E_1 \subset E_0$ is a generator of an analytic semigroup on E_0 and, moreover, $A_1 \in \mathcal{M}_1(E_0, E_1)$ (see [5]). Notice that $d_\alpha F(\bar{\Phi}, \bar{\alpha})$ belongs to $\mathcal{L}(C^{2+\varrho}(S^1), E_{\frac{1}{2}})$ and this is why we can write $d_\Phi f(\bar{\Phi})$ as a sum $A_1 + A_2$ where $A_2 \in L(E_{\frac{1}{2}}, E_0)$. Thus $\|A_2\Phi\|_{E_0} \leq C\|\Phi\|_{E_{\frac{1}{2}}} \leq C\|\Phi\|^{1/2}_{E_0}\|\Phi\|^{1/2}_{E_1}$ and so the linear operator A_2 is a relatively bounded linear perturbation of A_1 with zero relative bound (cf. [5]). With regard to [5, Lemma 2.5] the class $\mathcal{M}_1$ is closed with respect to such perturbations. Thus $d_\Phi f(\bar{\Phi}) \in \mathcal{M}_1(E_0, E_1)$. The proof of the short time existence of a solution Φ now follows from [5, Theorem 2.7].

Finally, we will show that the maximal curvature becomes unbounded as $t \to T_{max}$ in the case $\liminf_{t\to T^-_{max}} \min_{\Gamma_t} \beta'_k > 0$ and $T_{max} < +\infty$. Suppose to the contrary that $\max_{\Gamma_t} |k| \leq M < \infty$ for any $t \in [0, T_{max})$. According to [3, Theorem 3.1] there exists a unique maximal solution $\Gamma : [0, T'_{max}) \to \Omega(\mathbb{R}^2)$ satisfying the geometric Eq. (1.1). Recall that $\Omega(\mathbb{R}^2)$ is the space of C^1 regular Jordan curves in the plane (cf. [3]). Moreover, Γ_t is a C^∞ smooth curve for any $t \in (0, T'_{max})$ and the maximum of the absolute value of the curvature tends to infinity as $t \to T'_{max}$. Thus $T_{max} < T'_{max}$ and therefore the curvature and subsequently ν remain bounded in $C^{2+\varrho'}$ norm on the interval $[0, T_{max}]$ for any $\varrho' \in (\varrho, 1)$. Applying the compactness argument one sees that the limit $\lim_{t\to T_{max}} \Phi(., t)$ exists and remains bounded in the space E_1 and one can continue the solution Φ beyond T_{max}, a contradiction. □

Remark 3.2. In a general case where the normal velocity may depend on the position vector x, the maximal time of existence of a solution can be either finite or infinite. Indeed, as an example one can consider the unit ball $B = \{|x| < 1\}$ and function $\delta(x) = (|x| - 1)^\gamma$ for $x \notin B, \gamma > 0$. Suppose that $\Gamma_0 = \{|x| = R_0\}$ is a circle with a radius $R_0 > 1$ and the family $\Gamma_t, t \in [0, T)$, evolves according to the normal velocity function $\beta(x, k) = \delta(x)k$. Then, it is an easy calculus to verify that the family Γ_t approaches the boundary $\partial B = \{|x| = 1\}$ in a finite time $T_{max} < \infty$ provided that $0 < \gamma < 1$ whereas $T_{max} = +\infty$ in the case $\gamma = 1$.

4. Lyapunov functionals and qualitative properties of solutions. In this section we will analyze the qualitative properties of a solution to the governing system of Eqs. (3.2) – (3.5). The aim is to derive suitable Lyapunov functionals decreasing along trajectories as well as to prove *á-priori* estimates of solutions to (3.2) – (3.5) for particular choices of the normal velocity functional

We begin with a well-known identity for the total length of evolving curves satisfying (1.1). Since α is periodic in u variable we obtain from (3.4)

$$\frac{d}{dt}L_t + \int_{\Gamma_t} k\beta \, ds = 0 \qquad \text{where } L_t = \int_{\Gamma_t} ds = \int_0^1 g(u,t)\, du \tag{4.1}$$

is the total length of a curve Γ_t. If $k\beta \geq 0$ then the evolution of plane curves parameterized by a solution of (1.2) represents a curve shortening flow, i.e. $L_{t_2} \leq L_{t_1} \leq L_0$ for any $0 \leq t_1 \leq t_2 \leq T$.

In the rest of this section we will only focus on the normal velocity function β arising from the image segmentation problem discussed in more detail in section 2.2. We will assume the normal velocity function $v = \beta(x, k, \nu)$ has the following form:

$$\beta(x, k, \nu) = a(\phi)\, k - b(\phi)(\nabla\phi.\vec{N}) \tag{4.2}$$

where $\phi = \phi(x)$ is a smooth and bounded (up to the second derivative) function, $\phi : \Omega \to (0, 1]$ defined in a domain $\Omega \subset \mathbb{R}^2$ and $a = a(\phi), b = b(\phi)$ are smooth functions $a(\phi) > 0$ for $\phi > 0$.

Let us consider a flow $\Gamma_t, t \geq 0$, of plane curves with the normal velocity given by (4.2). Local in time existence of a smooth solution follows from Theorem 3.1 provided that the initial curve $\Gamma_0 \subset \Omega$ is smooth. Notice that

$$\phi(x) > 0 \quad \text{for any } x \in \Gamma_0 \,. \tag{4.3}$$

In the following proposition we will show that the flow $\Gamma_t, t \geq 0$, has a gradient structure, i.e. there exists a Lyapunov functional non-increasing with respect to time t.

PROPOSITION 4.1. *If a family Γ_t , $0 \leq t < T_{max}$, of plane curves satisfies (4.2) then*

$$\frac{d}{dt}\int_{\Gamma_t} H(\phi(x))\, ds + \int_{\Gamma_t} \frac{H(\phi(x))}{a(\phi(x))}\beta^2\, ds = 0\,, \quad \textit{where } H(\phi) = e^{\int_0^\phi \frac{b(\xi)}{a(\xi)}\, d\xi}\,. \tag{4.4}$$

In particular, the functional $V(\Gamma) = \int_\Gamma H(\phi(x))\, ds$ is a Lyapunov functional, i.e. $\frac{d}{dt}V(\Gamma_t) \leq 0$ for any $0 \leq t < T_{max}$.

Proof. Clearly,

$$\begin{aligned}
\partial_t H(\phi) = H'(\phi)(\nabla\phi.\partial_t x) &= \frac{bH(\phi)}{a}(\beta(\nabla\phi.\vec{N}) + \alpha(\nabla\phi.\vec{T})) \\
&= \frac{bH(\phi)}{a}\beta(\nabla\phi.\vec{N}) + \alpha\partial_s H(\phi)
\end{aligned}$$

where $\phi = \phi(x)$, $a = a(\phi)$, $b = b(\phi)$, and $x = x(u,t)$ is a solution to (3.2) – (3.5) representing the curve Γ_t, i.e. $\Gamma_t = \text{Image}(x(.,t))$. Since $ds = g du$ and $\partial_t g = -gk\beta + \partial_u\alpha$ we have

$$\begin{aligned}
\frac{d}{dt}\int_{\Gamma_t} H(\phi)\, ds &= \int_{\Gamma_t} \partial_t H(\phi) - H(\phi)k\beta + H(\phi)\partial_s\alpha\, ds \\
&= \int_{\Gamma_t} \beta H(\phi)\left(\frac{b}{a}(\nabla\phi.\vec{N}) - k\right) ds = -\int_{\Gamma_t} \frac{\beta^2}{a} H(\phi)\, ds
\end{aligned}$$

because $\beta = a\,k - b(\nabla\phi.\vec{N})$ and $\int_{\Gamma_t} \alpha\partial_s H + H\partial_s\alpha\, ds = \int_{\Gamma_t} \partial_s(\alpha H)\, ds = 0$. □

As an immediate consequence of the previous result we can exclude the existence of time periodic families of plane curves with normal velocity satisfying (4.2).

Corollary 4.1. There exists no nontrivial time periodic family of plane curves Γ_t , $t \geq 0$, satisfying (4.2).

The next result is focused on *á-priori* estimates of solutions. We will need the following structural assumptions made on the functions a and ϕ.

$$\begin{aligned}
&a(0) = 0\,,\ 0 < a(\phi) \leq C_1\phi\,, \quad \text{for any } 0 < \phi \leq 1\,, \\
&|\nabla\phi(x)| \leq C_2\phi(x) \quad \text{for any } x \in \Omega
\end{aligned} \tag{4.5}$$

where $C_1, C_2 > 0$ are positive constants. Notice that this hypothesis is fulfilled in the case $a(\phi) = \varepsilon\phi\,, \varepsilon > 0$ and the function ϕ is defined as in (2.6), i.e. $\phi(x) = h(|\nabla u_0(x)|)$ where h is an arbitrary edge detector function and u_0 is a smoothed image intensity function.

LEMMA 4.2. *Assume (4.5). If a family Γ_t , $0 \leq t < T_{max}$, of plane curves satisfies (4.2) then there exists a constant $C > 0$ such that*

$$\min_{x\in\Gamma_t} \phi(x) \geq e^{-Ct} \min_{x\in\Gamma_0} \phi(x)$$

for any $0 \le t < T_{max}$.

Proof. Let $z(u,t) = \phi(x(u,t))$ where $\Gamma_t = \text{Image}(x(.,t))$ and x is a solution to (3.2) – (3.5). With regard to (1.2) and Frenét's formulae it is an easy calculation to verify that z is a solution to the following parabolic equation:

$$\partial_t z = a(z)\partial_s^2 z - a(z)\vec{T}^T\nabla^2\phi\vec{T} + \alpha\partial_s z - b(z)(\nabla\phi.\vec{N})^2$$

where $a(z) = a(z(u,t)) \ge 0,\ b(z) = b(z(u,t))$. Since ϕ is assumed to be smooth it follows from (4.5) that there exist constants $C_3, C_4 > 0$ such that $|a(\phi(x))\vec{T}^T\nabla^2\phi(x)\vec{T}| \le C_3\phi(x) = C_3 z$ and $|b(\phi(x))||\nabla\phi(x)|^2 \le C_4\phi(x) = C_4 z$. Since $|\nabla\phi(x)|^2 = (\nabla\phi(x).\vec{N})^2 + (\nabla\phi(x).\vec{T})^2 = (\nabla\phi(x).\vec{N})^2 + (\partial_s z)^2$ we have

$$\partial_t z \ge a\partial_s^2 z + (b(z)\partial_s z + \alpha)\partial_s z - Cz$$

for some constant $C > 0$ depending only on C_3 and C_4. Applying the parabolic maximum principle yields

$$\min_{u\in[0,1]} z(u,t) \ge e^{-Ct}\min_{u\in[0,1]} z(u,0)$$

for any $0 \le t < T_{max}$ and the proof of lemma follows. □

As a consequence of the previous result we obtain

PROPOSITION 4.3. *Assume the hypothesis (4.5) is fulfilled. If the normal velocity of an evolving family* Γ_t , $0 \le t < T_{max}$, *of plane curves satisfies (4.2) then for the maximal time of existence of a solution we have either* $T_{max} = \infty$ *or* $T_{max} < \infty$. *If* $T_{max} < \infty$ *then modulus of the curvature* $|k(.,t)|$ *becomes unbounded and* $L_t \to 0$ *as* $t \to T_{max}$.

Proof. The proof follows from Theorem 3.1 and the previous lemma. □

5. Controlling the tangential motion. The purpose of this section is to discuss the role of a tangential velocity functional α in the position vector Eq. (1.2). In comparison to the approach developed [32] where an initial distribution of grid points is preserved during evolution the aim of this section is to generalize this approach in order to achieve uniform redistribution of points belonging to Γ_t.

The idea behind the construction of a suitable functional α is to examine the behavior of the so-called relative local length defined as the ratio $\frac{g(u,t)}{L_t}$. If this ratio tends to some constant $C > 0$ as $t \to T_{max}$, i.e. $\lim_{t\to T_{max}^-} \frac{g(u,t)}{L_t} = C$ then, at the maximal time $t = T_{max}$ the redistribution of grid points becomes constant. Inevitably, the identity $\int_0^1 g(u,t)\,du = L_t$ implies $C = 1$. Moreover, the condition

$$\lim_{t\to T_{max}^-} \frac{g(u,t)}{L_t} = 1$$

is fulfilled provided that there exists a relaxation function $\omega \in L^1_{loc}([0, T_{max}))$ such that

$$\int_0^{T_{max}} \omega(\tau)\,d\tau = \infty \qquad (5.1)$$

and $g(u,t)/L_t = 1 + (g_0(u)/L_0 - 1)\,e^{-\int_0^t \omega(\tau)\,d\tau}$ for any $u \in [0,1]$ and $t \in [0, T_{max})$. This equation can be rewritten as an ODE

$$\frac{d}{dt}\left(\frac{g(u,t)}{L_t} - 1\right) + \omega(t)\left(\frac{g(u,t)}{L_t} - 1\right) = 0\,.$$

Taking into account the local length equation (3.4) and total length Eq. (4.1) the above ODE is satisfied if and only if the tangential velocity functional α obeys the equation

$$\partial_u \alpha = g\left(k\beta - \frac{1}{L}\int_\Gamma k\beta\right) + \omega(t)(L-g) \tag{5.2}$$

where $L = L_t$ is the total length of the curve $\Gamma = \Gamma_t$.

5.1. Finite time extinction solutions. By a finite time extinction solution the mean curvature flow we mean an evolving family of plane curves Γ_t existing on a maximal finite time interval $[0, T_{max})$ where $T_{max} < \infty$ and such that the total length L_t vanishes as $t \to T_{max}^-$, i.e. $\lim_{t\to T_{max}^-} L_t = 0$. It is always the case if the normal velocity β satisfies

$$\beta'_k(x,k,\nu) \ge \lambda, \quad \beta(x,0,\nu) = 0$$

for any x, k, ν where $\lambda > 0$ is a constant. As an example one can consider the normal velocity of the form $\beta(x,k,\nu) = \delta(x,\nu)k$ where $\delta \ge \lambda > 0$.

Let us define a relaxation function ω as follows:

$$\omega(t) = \frac{\kappa}{L_t}\int_{\Gamma_t} k\beta\, ds \tag{5.3}$$

where $\kappa > 0$ is a positive constant. According to (4.1) we have

$$\int_0^t \omega(\tau)\, d\tau = -\kappa\int_0^t \partial_\tau \ln L_\tau d\tau = \kappa(\ln L_0 - \ln L_t) \to \infty \quad \text{as } t \to T_{max}^- .$$

Hence the relaxation function ω defined by (5.3) satisfies the structural condition (5.1). In this case Eq. (5.2) has the form

$$\partial_u \alpha = g\left(k\beta - \frac{1+\kappa}{L}\int_\Gamma k\beta\right) + \kappa\int_\Gamma k\beta\, . \tag{5.4}$$

Remark 5.1. If we formally set $\kappa = 0$ in (5.4) then we obtain the same equation for the tangential velocity α as the one derived in [32, Eq. (6.2)]. Recall that in this case the relative local length $g(u,t)/L_t$ is preserved, i.e. $g(u,t)/L_t = g_0(u)/L_0$ for any $u \in [0,1]$ and $t \in [0,T)$. On the other hand, taking $\kappa > 0$ yields $\lim_{t\to T_{max}^-} \frac{g(u,t)}{L_t} = 1$ for any $u \in [0,1]$ independently of the initial redistribution of the local length $g_0 = |\partial_u x_0|$ at $t = 0$.

5.2. Image segmentation problem. In this section we will study the case where the normal velocity function β arises from the image segmentation problem discussed in a more detail in sections 2.2 and 4. We will suppose that the normal velocity function $v = \beta(x,k,\nu)$ has the form (4.2) with coefficients a, b and the structural hypothesis (4.5) is satisfied.

Let $\Gamma_t, 0 \le t < T_{max}$, be a solution to (1.1) existing on a maximal time interval $[0, T_{max})$. With regard to Proposition 4.3 either $T_{max} = \infty$ or $T_{max} < \infty$. In the case $T_{max} < \infty$ we furthermore have $L_t \to 0$ as $t \to T_{max}^-$ and the function $\omega(t)$ defined as in (5.3) is a relaxation function. In the general case $T_{max} \le \infty$ let us define a function

$$\omega(t) = \kappa_1 + \frac{\kappa_2}{L_t}\int_{\Gamma_t} k\beta\, ds \tag{5.5}$$

where $\kappa_1, \kappa_2 > 0$ are some positive constants. In order to clarify how κ_1 must be chosen with respect to κ_2 let us denote $B(\phi)$ a primitive function to $b(\phi)$, i.e. $B'(\phi) = b(\phi)$. From Frenet's formula $\partial_s \vec{T} = k\vec{N}$ we have

$$-\int_{\Gamma_t} b(\phi(x))(\nabla\phi(x).\vec{N})k\, ds \; = -\int_{\Gamma_t} (\nabla B(\phi(x)).\partial_s \vec{T})\, ds$$

$$= \int_{\Gamma_t} \vec{T}^T \nabla^2 B(\phi(x)) \vec{T}\, ds \geq -C \int_{\Gamma_t} ds = -C\, L_t$$

where $C > 0$ is a constant such that $\max_{x\in\Omega} |\nabla^2 B(\phi(x))| \leq C$. Since

$$\int_{\Gamma_t} k\beta\, ds = \int_{\Gamma_t} a(\phi(x))\, k^2 - b(\phi(x))(\nabla\phi(x).\vec{N})k\, ds \geq -C\, L_t$$

we have $\int_0^{T_{max}} \omega(t)\, dt = \infty$ provided that $\kappa_1 > C\kappa_2$ irrespective of the fact whether $T_{max} < \infty$ or $T_{max} = \infty$. Hence ω can be used as a relaxation function.

PROPOSITION 5.1. *Up to an additive constant there exists a unique tangential velocity functional α satisfying (5.2) where the relaxation function ω given by (5.5) with $\kappa_1, \kappa_2 \geq 0$. Moreover, $\alpha \in C^1(\mathcal{O}_{\frac{1}{2}}, c^{2+\varrho}(S^1))$ i.e. the tangential velocity functional α satisfies the condition (3.8).*

Proof. The proof directly follows from definition of the tangential velocity functional α (5.2) and basic properties of Hölder spaces. □

6. Numerical scheme and computational results. The goal of this section is to describe a numerical algorithm we used for computing the curve evolution satisfying the geometric equation (1.1). We focus on a particular choice of the normal velocity satisfying (2.1) in which case the dependence of β on the curvature k is linear. In subsections 6.1 and 6.2 we present results for isotropic and anisotropic curve evolution with a constant driving force c and the anisotropy coefficient δ depending on the tangential angle ν only. Such a model plays an important role in the theory of interfacial thermomechanics and represents Angenent-Gurtin's approach to plane phase interface motion. In this case we solve numerically Eqs. (3.2) – (3.4) for the curvature, tangential angle and local length. Using these computed geometrical quantities, the position vector of the evolving curve is reconstructed afterwards. In subsection 6.3, we present the algorithm for the curve evolution with a general, position dependent, driving force given e.g. by a vector field projected to the normal. In this general case, we replace (3.5) by an intrinsic convection-diffusion equation for the curve position vector x and solve also this equation numerically. In subsections 6.4 and 6.5 we discuss computational results obtained and we apply the method to the image segmentation problem described in section 2.2.

6.1. The scheme for an anisotropic curvature driven motion with a constant driving force. In this subsection we propose a numerical scheme for solving the initial value problem for the system of intrinsic Eqs. (3.2) – (3.4) for the curvature k, tangential angle ν and local length g. We consider the normal velocity of the form

$$\beta = \beta(k,\nu) = \gamma(\nu)k + F \tag{6.1}$$

with a given anisotropy function $\gamma(\nu) > 0$ and a constant driving force F. The system of governing equations is accompanied with the tangential velocity α given by

$$\partial_s \alpha = k\beta - \frac{1}{L}\int_\Gamma k\beta ds - \omega(1 - \frac{L}{g}) \tag{6.2}$$

where L is the total length of the curve Γ and ω is a relaxation function discussed in section 5. Then the evolving curve Γ_t itself is given (uniquely up to a translation) by the reconstruction formula:

$$x(u^*, .) = \int_0^{u^*} g\vec{T} du = \int_0^{s^*} \vec{T} ds \tag{6.3}$$

where $s^* = s(u^*)$ is a time dependent arc-length parameter corresponding to the fixed domain spatial parametrization u. A discrete version of such a reconstruction will be used in the numerical scheme.

Before performing temporal and spatial discretization we insert (6.2) into (3.2) and (3.4) to obtain

$$\partial_t k = \partial_s^2 \beta + \partial_s(\alpha k) + k\frac{1}{L}\int_\Gamma k\beta ds + k\omega(1-\frac{L}{g}), \tag{6.4}$$

$$\partial_t \nu = \beta'_k \partial_s^2 \nu + (\alpha + \beta'_\nu)\partial_s \nu\,, \tag{6.5}$$

$$\partial_t g = -g\frac{1}{L}\int_\Gamma k\beta ds - \omega(g-L). \tag{6.6}$$

From the numerical discretization point of view, critical terms in Eqs. (3.2) – (3.4), are represented by the reaction term $k^2\beta$ in (3.2) and the decay term $k\beta$ in (3.4). In Eqs. (6.4) – (6.6) these critical terms were replaced by the averaged value of $k\beta$ along the curve. A possible bad pointwise influence of these terms is therefore weakened and the computation of a local element length in the neighborhood of point with a high curvature is more stable. A numerical scheme can benefit from this property as it allows for larger time steps without loss of stability.

In our computational method a solution of the evolution Eq. (1.1) is represented by discrete plane points $x_i^j, i = 0, ..., n,\ j = 0, ..., m$, where index i represents space discretization and index j a discrete time stepping. The approximation of an evolving curve in j-th discrete time step is thus given by a polygon with vertices $x_i^j, i = 0, ..., n$. Since we only consider closed initial curves the periodicity condition $x_0^0 = x_n^0$ is required at the beginning. If we take a uniform division of the time interval $[0, T]$ with a time step $\tau = \frac{T}{m}$ and a uniform division of the fixed parametrization interval $[0, 1]$ with a step $h = \frac{1}{n}$, a point x_i^j corresponds to $x(ih, j\tau)$. It is worthwhile noting that due to the intrinsic character of the governing equations a spatial discretization step h does not appear in the numerical scheme. In order to construct the approximation of an evolving curve we will derive systems of difference equations corresponding to (6.4) – (6.6) which are solved at every discrete time step. Difference equations will be given for discrete quantities $k_i^j, \nu_i^j, r_i^j, i = 1, ..., n,\ j = 1, ..., m$ representing piecewise constant approximations of the curvature, tangent angle and element length for the segment $\left[x_{i-1}^j, x_i^j\right]$. Then, at the j-th discrete time level, $j = 1, ..., m$, approximation of a curve is given by a discrete version of the reconstruction formula

$$x_i^j = x_0^j + \sum_{l=1}^{i} r_l^j(\cos(\nu_l^j), \sin(\nu_l^j)),\ \ i = 1, ..., n. \tag{6.7}$$

Since the reconstruction is unique up to a translation, i.e. a position of the point x_0^j we have to track the evolution of this point by a straightforward way using (1.2) with zero tangential velocity (see also (6.9))

$$x_0^j = x_0^{j-1} + \tau\beta((k_1^j + k_n^j)/2, (\nu_1^j + \nu_n^j)/2). \tag{6.8}$$

It is worth to note that the periodic boundary condition $x_0^j = x_n^j, j > 0$, is not automatically satisfied when using (6.7). It depends on how precisely all the discrete quantities are computed by the scheme. From the presented numerical experiments (Figures 5.1-5.9 below) one can see that the difference of computed endpoints x_0^j and x_n^j is sufficiently small in numerical solutions.

Our algorithm is semi-implicit in time, i.e., all non-linear terms are treated from the previous time step and discretization leads to a solution of linear systems of equations at every discrete time level. At the j-th time step, $j = 1, .., m$, we first find discrete values of the tangential velocity functional α_i^j. Then new discrete local lengths r_i^j are computed and finally two tridiagonal systems with periodic boundary conditions are solved for the discrete curvature k_i^j and discrete tangent angle ν_i^j.

In order to construct a discretization scheme for solving (6.4) – (6.6) we will consider time dependent functions $k_i(t), \nu_i(t), r_i(t)$ representing constant approximation of k, ν, gh in a flowing-in-time linear segment $[x_{i-1}(t), x_i(t)]$. The function $\alpha_i(t)$ will represent tangential velocity of a flowing node $x_i(t)$. The values k_i^j, ν_i^j, r_i^j, x_i^j, described above then represent approximations of the time dependent functions at time level $t = j\tau$. In the sequel, the parameter t will be omitted. Let us denote $B = \frac{1}{L}\int_\Gamma k\beta ds$. We integrate Eqs. (6.4) – (6.6) and (6.2) over the so-called *flowing control volume* $[x_{i-1}, x_i]$. At any time t, for the tangential velocity functional α we have

$$\int\limits_{x_{i-1}}^{x_i} \partial_s \alpha ds = \int\limits_{x_{i-1}}^{x_i} k\beta - B - \omega\left(1 - \frac{L}{g}\right) ds,$$
$$\alpha_i - \alpha_{i-1} = r_i k_i \beta(k_i, \nu_i) - r_i B - \omega\left(r_i - \frac{L}{n}\right).$$

By taking discrete time stepping in the previous relation, for *discrete values of the tangential velocity functional* α_i^j we obtain

$$\alpha_i^j = \alpha_{i-1}^j + r_i^{j-1} k_i^{j-1} \beta(k_i^{j-1}, \nu_i^{j-1}) - r_i^{j-1} B^{j-1} - \omega(r_i^{j-1} - M^{j-1}), \quad i = 1, ..., n, \ \text{ with } \alpha_0^j = 0 \tag{6.9}$$

(according to (6.8) the point x_0^j is moving only in the normal direction) where

$$M^{j-1} = \frac{1}{n} L^{j-1}, \ \ L^{j-1} = \sum_{l=1}^n r_l^{j-1} \tag{6.10}$$

are the average of element lengths and discrete length of the curve, respectively,

$$B^{j-1} = \frac{1}{L^{j-1}} \sum_{l=1}^n r_l^{j-1} k_l^{j-1} \beta(k_l^{j-1}, \nu_l^{j-1}), \tag{6.11}$$

and

$$\omega = \kappa_1 + \kappa_2 B^{j-1}, \tag{6.12}$$

with input redistribution parameters κ_1, κ_2. Concerning discretization of Eq. (6.6) we proceed along the following lines:

$$\int\limits_{x_{i-1}}^{x_i} \partial_t g ds = -\int\limits_{x_{i-1}}^{x_i} gB + \omega\left(g - L\right) ds,$$
$$r_i \frac{1}{h}\frac{dr_i}{dt} + r_i \frac{r_i}{h} B + r_i \frac{r_i}{h}\omega = r_i \omega L\,,$$
$$\frac{dr_i}{dt} + r_i B + r_i \omega = \omega \frac{L}{n}\,.$$

By replacing the time derivative by time difference we obtain a semi-implicit *update for local lengths*

$$r_i^j = \frac{r_i^{j-1} + \tau\omega M^{j-1}}{1+\tau(B^{j-1}+\omega)}, \quad i=1,...,n, \quad r_0^j = r_n^j, \quad r_{n+1}^j = r_1^j. \tag{6.13}$$

Subsequently, new local lengths are used for approximation of intrinsic derivatives in (6.4) – (6.5). First, we derive a discrete analogy of the curvature Eq. (6.4). We have

$$\int_{x_{i-1}}^{x_i} \partial_t k ds = \int_{x_{i-1}}^{x_i} \partial_s^2 \beta(k,\nu) ds + \int_{x_{i-1}}^{x_i} \partial_s(\alpha k) ds + \int_{x_{i-1}}^{x_i} kB ds + \int_{x_{i-1}}^{x_i} k\omega\left(1-\frac{L}{g}\right) ds,$$

$$r_i \frac{dk_i}{dt} = [\partial_s \beta(k,\nu)]_{x_{i-1}}^{x_i} + [\alpha k]_{x_{i-1}}^{x_i} + k_i(r_i(B+\omega) - \omega\frac{L}{n}).$$

Now, by replacing the time derivative by time difference, approximating k in nodal points by the average value of neighboring segments, taking all linear terms at the new time level j and taking all the remaining terms from the previous time level $j-1$ we obtain a discretization scheme

$$r_i^j \frac{k_i^j - k_i^{j-1}}{\tau} = \frac{\gamma(\nu_{i+1}^{j-1})k_{i+1}^j - \gamma(\nu_i^{j-1})k_i^j}{q_i^j} - \frac{\gamma(\nu_i^{j-1})k_i^j - \gamma(\nu_{i-1}^{j-1})k_{i-1}^j}{q_{i-1}^j} +$$
$$\alpha_i^j \frac{k_{i+1}^j + k_i^j}{2} - \alpha_{i-1}^j \frac{k_i^j + k_{i-1}^j}{2} + k_i^j(r_i^j(B^{j-1}+\omega) - \omega M^{j-1}),$$
$$\text{where } q_i^j = \frac{r_i^j + r_{i+1}^j}{2}, \quad i=1,...,n.$$

In other words, we use central differences for approximations of first order terms. Other possibilities like up-winding could be also possible, but we do not follow this approach in our implementation. Collecting corresponding terms we end up with a *tridiagonal system* with periodic boundary conditions imposed *for new discrete values of curvature*, i.e.

$$a_i^j k_{i-1}^j + b_i^j k_i^j + c_i^j k_{i+1}^j = d_i^j, \quad i=1,...,n, \quad k_0^j = k_n^j, \quad k_{n+1}^j = k_1^j, \tag{6.14}$$

where

$$a_i^j = \frac{\alpha_{i-1}^j}{2} - \frac{\gamma(\nu_{i-1}^{j-1})}{q_{i-1}^j},$$
$$b_i^j = r_i^j\left(\frac{1}{\tau} - (B^{j-1}+\omega)\right) + \omega M^{j-1} - \frac{\alpha_i^j}{2} + \frac{\alpha_{i-1}^j}{2} + \frac{\gamma(\nu_i^{j-1})}{q_{i-1}^j} + \frac{\gamma(\nu_i^{j-1})}{q_i^j},$$
$$c_i^j = -\frac{\alpha_i^j}{2} - \frac{\gamma(\nu_{i+1}^{j-1})}{q_i^j},$$
$$d_i^j = \frac{r_i^j}{\tau} k_i^{j-1}.$$

Finally, we solve the tangent angle Eq. (6.5) using the following approximation:

$$\int_{x_{i-1}}^{x_i} \partial_t \nu ds = \beta_k'(k_i,\nu_i)\int_{x_{i-1}}^{x_i} \partial_s^2 \nu ds + \int_{x_{i-1}}^{x_i} \alpha\partial_s \nu ds + \beta_\nu'(k_i,\nu_i)\int_{x_{i-1}}^{x_i} \partial_s \nu ds,$$

$$r_i \frac{d\nu_i}{dt} = \gamma(\nu_i)\left[\partial_s \nu\right]_{x_{i-1}}^{x_i} + [\alpha\nu]_{x_{i-1}}^{x_i} - \nu_i \int_{x_{i-1}}^{x_i} \partial_s \alpha ds + \gamma'(\nu_i)k_i\left[\nu\right]_{x_{i-1}}^{x_i}.$$

Again, values of ν in nodal points are approximated by the average of neighboring segments values, the time derivative is replaced by the time difference. We use a semi-implicit approach to obtain

$$r_i^j \frac{\nu_i^j - \nu_i^{j-1}}{\tau} = \gamma(\nu_i^{j-1}) \left(\frac{\nu_{i+1}^j - \nu_i^j}{q_i^j} - \frac{\nu_i^j - \nu_{i-1}^j}{q_{i-1}^j} \right) +$$
$$\alpha_i^j \frac{\nu_{i+1}^j + \nu_i^j}{2} - \alpha_{i-1}^j \frac{\nu_i^j + \nu_{i-1}^j}{2} - \nu_i^j(\alpha_i^j - \alpha_{i-1}^j) + \gamma'(\nu_i^{j-1}) k_i^j \left(\frac{\nu_{i+1}^j - \nu_{i-1}^j}{2} \right).$$

Collecting the corresponding terms we again end up with a *tridiagonal system* with periodic boundary conditions *for new values of the tangent angle*

$$A_i^j \nu_{i-1}^j + B_i^j \nu_i^j + C_i^j \nu_{i+1}^j = D_i^j, \ \ i = 1, ..., n, \ \ \nu_0^j = \nu_n^j, \ \ \nu_{n+1}^j = \nu_1^j, \tag{6.15}$$

where

$$\begin{aligned} A_i^j &= \frac{\alpha_{i-1}^j}{2} + \frac{\gamma'(\nu_i^{j-1}) k_i^j}{2} - \frac{\gamma(\nu_i^{j-1})}{q_{i-1}^j}, \\ B_i^j &= \frac{r_i^j}{\tau} - (A_i^j + C_i^j), \\ C_i^j &= -\frac{\alpha_i^j}{2} - \frac{\gamma'(\nu_i^{j-1}) k_i^j}{2} - \frac{\gamma(\nu_i^{j-1})}{q_i^j}, \\ D_i^j &= \frac{r_i^j}{\tau} \nu_i^{j-1}. \end{aligned}$$

The initial quantities for the algorithm are computed as follows:

$$R_i = (R_{i_1}, R_{i_2}) = x_i^0 - x_{i-1}^0, \ \ i = 1, ..., n, \ \ R_0 = R_n, \ \ R_{n+1} = R_1,$$
$$r_i^0 = |R_i|, \ \ i = 0, ..., n+1, \tag{6.16}$$
$$k_i = \frac{1}{2 r_i^0} \mathrm{sgn}(R_{i-1} \wedge R_{i+1}) \arccos \left(\frac{R_{i+1} . R_{i-1}}{r_{i+1}^0 r_{i-1}^0} \right), \tag{6.17}$$
$$i = 1, ..., n, \ k_0^0 = k_n^0, \ k_{n+1}^0 = k_1^0,$$
$$\nu_0^0 = \arccos(R_{i_1}/r_i^0) \text{ if } R_{i_2} \geq 0, \ \ \nu_0^0 = 2\pi - \arccos(R_{i_1}/r_i) \text{ if } R_{i_2} < 0,$$
$$\nu_i^0 = \nu_{i-1}^0 + r_i^0 k_i^0, \ \ i = 1, ..., n+1. \tag{6.18}$$

Remark 6.1 (*Solvability and stability of the scheme.*) Let us first examine discrete values of the tangent angle computed from (6.15). One can rewrite it into the form

$$\nu_i^j + \frac{\tau}{r_i^j} C_i^j (\nu_{i+1}^j - \nu_i^j) + \frac{\tau}{r_i^j} A_i^j (\nu_{i-1}^j - \nu_i^j) = \nu_i^{j-1}. \tag{6.19}$$

Let $\max_k \nu_k^j$ be attained at the i-th node. We can always take a fine enough resolution of the curve, i.e. take small $q_i^j \ll 1$, $i = 1, .., n$, such that both A_i^j and C_i^j are nonpositive and thus the second and third terms on the left hand side of (6.19) are nonnegative. Then $\max_k \nu_k^j = \nu_i^j \leq \nu_i^{j-1} \leq \max_k \nu_k^{j-1}$. By a similar argument we can derive an inequality for minimum. In this way we have shown the L^∞-stability criterion, namely

$$\min_k \nu_k^0 \leq \min_k \nu_k^j \leq \max_k \nu_k^j \leq \max_k \nu_k^0, \ \ j = 1, .., m. \tag{6.20}$$

Having guaranteed nonpositivity of A_i^j and C_i^j we can conclude positivity and diagonal dominance of the diagonal term B_i^j. In particular, it implies that the tridiagonal matrix of the system (6.15) is an M-matrix and hence a solution to (6.15) always exists and is unique.

In the same way, by taking q_i^j small enough, we can prove nonpositivity of the off-diagonal terms a_i^j and c_i^j in the system (6.14) for discrete curvature values. Then the diagonal term b_i^j is positive and dominant provided that $\tau(B^{j-1}+\omega) < 1$. Again we have shown that the corresponding matrix is an M-matrix and therefore there exists a unique solution to the system (6.14).

Another natural stability requirement of the scheme is related to the positivity of local lengths r_i^j during computations. It follows from (6.13) that the positivity of r_i^j is equivalent to the condition $\tau(B^{j-1}+\omega) > -1$. Taking into account both inequalities for the time step we end up with the following stability restriction on the time step τ:

$$\tau \le \frac{1}{|B^{j-1}+\omega|} \tag{6.21}$$

related to B^{j-1} (a discrete average value of $k\beta$ over a curve).

6.2. Computational results for isotropic and anisotropic curve evolution with a constant driving force. In Figures 6.1-6.9 to follow we present numerical solutions computed by the scheme given in the previous subsection for the case $v = \beta(k,\nu) = \gamma(\nu)k + F$. In all figures of this subsection and subsection 6.4, initial curves are plotted with a thick line and the numerical solution is given by further solid lines with points representing the motion of some grid points during the curve evolution. As an initial curve for computation presented in Figures 6.1-6.3, Figure 6.8 left and Figures 6.10-6.13 we chose $x_1(u) = \cos(2\pi u)$, $x_2(u) = 2\sin(2\pi u) - 1.99\sin^3(2\pi u)$, $u \in [0,1]$. In Figures 6.4-6.5 we have considered an initial curve $x_1(u) = (1 - C\cos^2(2\pi u))\cos(2\pi u)$, $x_2(u) = (1 - C\cos^2(2\pi u))\sin(2\pi u)$, $u \in [0,1]$ with $C = 0.7$, and in Figure 6.6 the same curve with $C = 0.5$. In Figure 6.7 and Figure 6.8 right, we start with $x_1(u) = \frac{1}{2}\cos(2\pi u)$, $x_2(u) = \frac{3}{4}(\sin(2\pi u) + 0.8\sin(2x_1^2(u)) + 0.2\sin(3\exp(-x_1(u))) + \sin(2\pi u)(0.2 + \sin(2\pi u)\sin^2(6\pi u)))$, $u \in [0,1]$. In Figure 6.9 we start with a unit circle. In all presented experiments including redistribution in this subsection, the parameters $\kappa_1 = \kappa_2 = 10$.

We considered the isotropic case where $\gamma(\nu) = \varepsilon \equiv \mathrm{const} > 0$. Computations were performed for various values of a parameter ε and driving force F. In Figure 6.1 we present inner and outer curve evolutions for the time step $\tau = 0.0001$. In both cases, we plot each $100th$ discrete step and curves are represented by 800 grid points (left) and by 400 grid points (right), respectively. In Figures 6.2, 6.3 we compare computations with and without tangential redistribution with a larger driving force F. Without redistribution, the computations are collapsing soon because of the degeneracy in local element lengths in parts of a curve with high curvature leading to a merging of the corresponding grid points. Using the redistribution even the extreme case $F = 100$ and $\varepsilon = 1$ can be successfully handled and the resolution of sharp corners and their evolution is also possible. In this case convective terms related to redistribution dominate other terms in (6.4) – (6.5). Since we have used the most simple discretization (central differences) we had to increase a number of grid points in order to ensure stability related to the M-matrix property of the tridiagonal systems (6.14) and (6.15) discussed in Remark 6.1. It is natural that we have to use small time steps in case of such a strong driving force. However, the time step is not restricted by the point-wise values of the almost singular curvature in the corners which would lead to an un-realistic time step restriction. According to (6.21), the time step is restricted by the average value of $k\beta$ computed over the curve which is much more weaker restriction because of the regularity of the

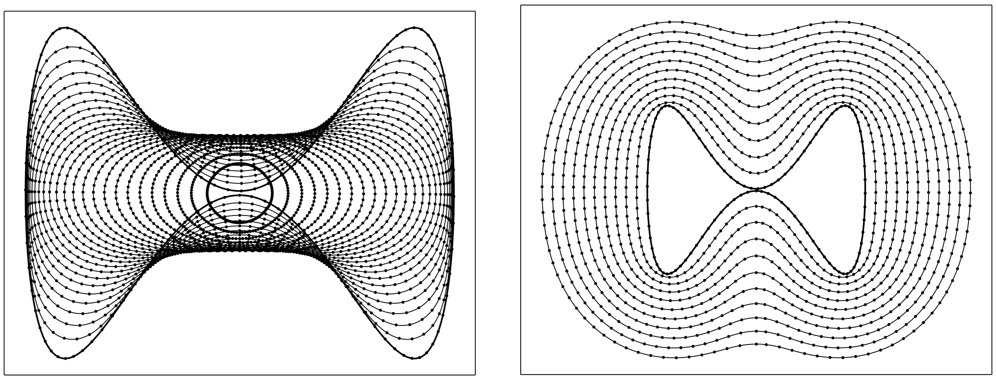

FIG. 6.1. *Isotropic curvature driven motion of an initial nonconvex curve including uniform tangential redistribution of grid points;* $\beta(k,\nu) = \varepsilon k + F$, *with* $\varepsilon = 1$, $F = 0$ *(left) and* $\varepsilon = 1$, $F = -10$ *(right).*

curve outside the corners. In Figure 6.2 we used $\tau = 0.00001$, 400 discrete grid points and we plotted every $150th$ time step. In Figure 6.3, $\tau = 0.000001$, we used 4000 discrete grid points and plotted every $300th$ time step.

In Figures 6.4-6.6 we present computations starting with another nonconvex initial curve. We show its evolution without and with a driving force F, with sharp corners formation and also with anisotropy. For computations depicted in Figures 6.4-6.5 we took $\tau = 0.00001$ and there were 400 (Figure 6.4 left), 800 (Figure 6.4 right, Figure 6.5 left) and 1600 (Figure 6.5 right) grid points for representation of a curve. In Figure 6.4 left we plotted each $1000th$ step, in Figures 6.4 right and 6.5 left each $500th$ time step, and in Figure 6.5 right each $100th$ step. The anisotropic experiment shown in Figure 6.6 was computed using $\tau = 0.00001, 4000$ grid points and we plotted every 500th time step.

In Figure 6.7 we used $\tau = 0.00001$ and 2000 grid points. In the left figure we computed 65000 time steps and plotted every $5000th$ step. In the right one we computed 5000 time steps and plotted every $1000th$. Two anisotropic experiments corresponding to Figure 6.1 left and Figure 6.7 right are shown in Figure 6.8. In the left figure we chose $\tau = 0.00001$, 1000 grid points and we plotted every $200th$ time step. In the right figure we chose $\tau = 0.00001, 5000$ grid points and we plotted every $1000th$ time step.

In Figure 6.9 we present experiments with three-fold anisotropy. We used $\tau = 0.001, 300$ grid points and we plotted every $50th$ time step (left) and every $750th$ time step (right). For the left experiment the theoretical blow-up time of the curvature is 0.5 whereas the computed one is approximately equal to 0.502.

Although the number of grid points for representation of a curve might be seen as rather large in some of the previous experiments, solving tridiagonal systems in each time step is still a fast and simple procedure.

6.3. A scheme for a mean curvature motion with a position dependent driving force. Since we consider (1.1) with a linear dependence of β on the curvature (2.1) by using Frenet's formulae one can rewrite the position vector Eq. (3.5) as an intrinsic convection-diffusion equation for the vector x

$$\partial_t k = \partial_s^2 \beta + \partial_s(\alpha k) + k\frac{1}{L}\int_\Gamma k\beta ds + k\omega(1 - \frac{L}{g}) \,, \tag{6.22}$$

$$\partial_t \nu = \beta'_k \partial_s^2 \nu + (\alpha + \beta'_\nu)\partial_s \nu + \nabla_x \beta . \vec{T} \,, \tag{6.23}$$

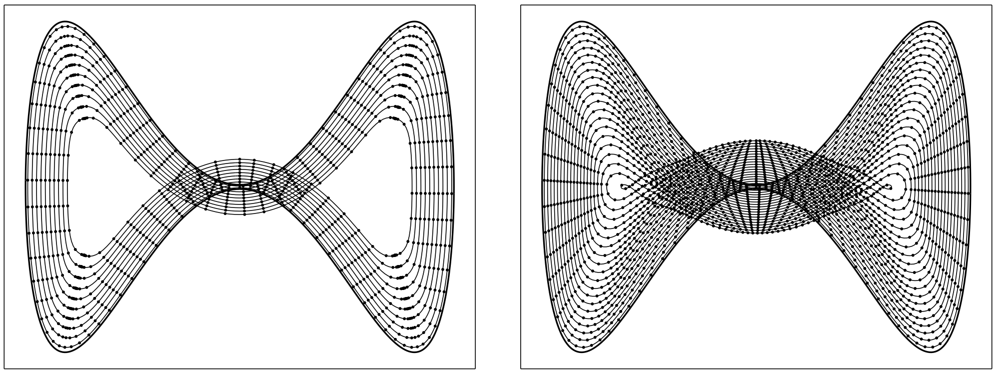

FIG. 6.2. *Isotropic curvature driven motion, $\beta(k,\nu) = \varepsilon k + F$, with $\varepsilon = 1$, $F = 10$, without (left) and with (right) uniform tangential redistribution of grid points.*

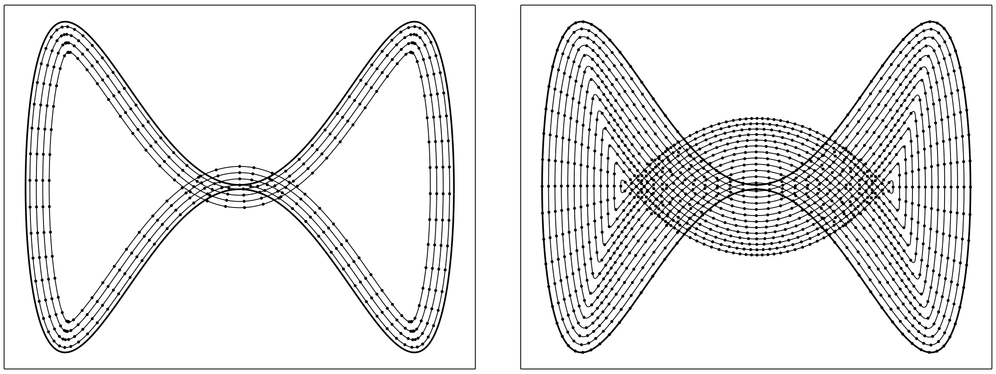

FIG. 6.3. *Isotropic curvature driven motion, $\beta(k,\nu) = \varepsilon k + F$, with $\varepsilon = 1$, $F = 100$, without (left) and with (right) uniform tangential redistribution of grid points. Resolution of sharp corners is possible using the algorithm with redistribution.*

$$\partial_t g = -g\frac{1}{L}\int_\Gamma k\beta ds - \omega(g-L)\,, \tag{6.24}$$

$$\partial_t x = \delta(x,\nu)\partial_s^2 x + \alpha\partial_s x + \vec{c}(x,\nu)\,, \tag{6.25}$$

where $\beta = \beta(x,k,\nu) = \delta(x,\nu)k + c(x,\nu)$ and $\vec{c}(x,\nu) = (-c(x,\nu)\sin\nu, c(x,\nu)\cos\nu)$. In comparison to the scheme analyzed in subsection 6.1, two new tridiagonal systems have to be solved at each time level in order to update the curve position vector x. The curve position itself and all geometric quantities entering the model are resolved from their own intrinsic Eqs. (6.22) – (6.25).

In order to construct a discretization scheme for (6.22) – (6.25) we can proceed in a similar way as in subsection 6.1 so we skip some details. Again, Eqs. (6.22) – (6.24) together with (6.2) are integrated over a flowing control volume $[x_{i-1}, x_i]$ and then semi-implicit in time approximations are employed. We also construct a time dependent dual volume $[\tilde{x}_{i-1}, \tilde{x}_i]$ where $\tilde{x}_i = \frac{x_{i-1}+x_i}{2}$ over which the last Eq. (6.25) will be integrated. Values $\tilde{x}_i^j, i = 1,..,n, j = 1,..,m$, represent time stepping of $\tilde{x}_i, i = 1,..,n$. For *discrete values of*

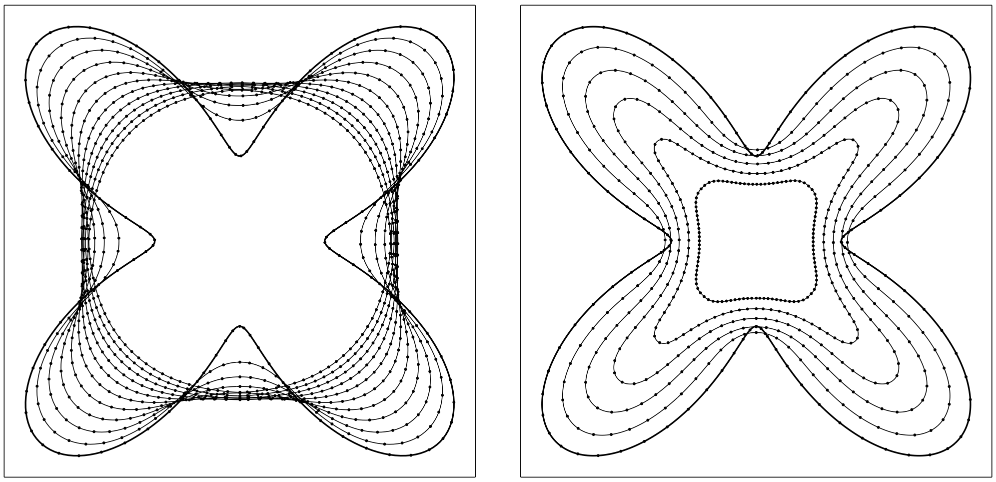

FIG. 6.4. *Isotropic curvature driven motion of an initial nonconvex curve including uniform tangential redistribution of grid points;* $\beta(k,\nu) = \varepsilon k + F$, *with* $\varepsilon = 1$, $F = 0$ *(left) and* $\varepsilon = 1$, $F = 10$ *(right).*

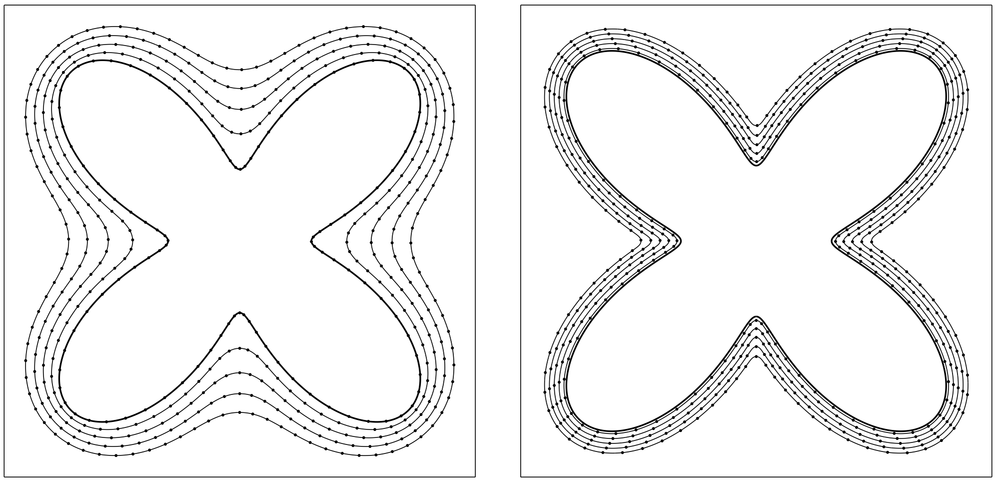

FIG. 6.5. *Isotropic curvature driven motion of an initial nonconvex curve including uniform tangential redistribution of grid points;* $\beta(k,\nu) = \varepsilon k + F$, *with* $\varepsilon = 1$, $F = -10$ *(left) and* $\varepsilon = 0.1$, $F = -10$ *(right). Resolution of sharp corners in the case of a highly dominant forcing term using the algorithm with redistribution is possible.*

the tangential velocity functional α_i^j we obtain

$$\begin{aligned}\alpha_i^j &= \alpha_{i-1}^j + r_i^{j-1} k_i^{j-1} \beta(\tilde{x}_i^{j-1}, k_i^{j-1}, \nu_i^{j-1}) - r_i^{j-1} B^{j-1} \\ &\quad - \omega(r_i^{j-1} - M^{j-1}), \ \ i = 1, ..., n, \ \ \alpha_0^j = 0,\end{aligned} \tag{6.26}$$

with M^{j-1}, L^{j-1}, ω given as in subsection 6.1 and

$$B^{j-1} = \frac{1}{L^{j-1}} \sum_{l=1}^{n} r_l^{j-1} k_l^{j-1} \beta(\tilde{x}_l^{j-1}, k_l^{j-1}, \nu_l^{j-1}). \tag{6.27}$$

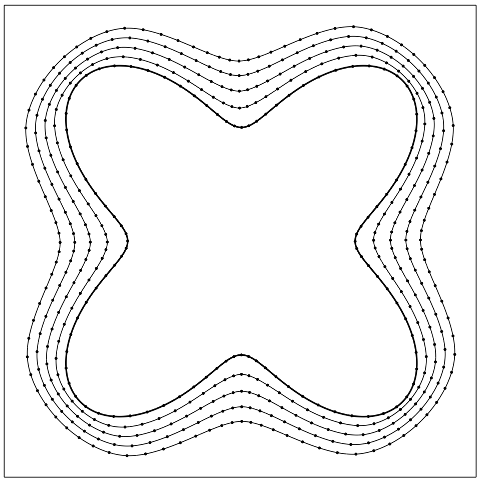

FIG. 6.6. *Anisotropic curvature driven motion of an initial nonconvex curve including uniform tangential redistribution of grid points;* $\beta(k,\nu) = \gamma(\nu)k + F$, *with* $\gamma(\nu) = 1 - 0.6\cos(4\nu)$, $F = -10$.

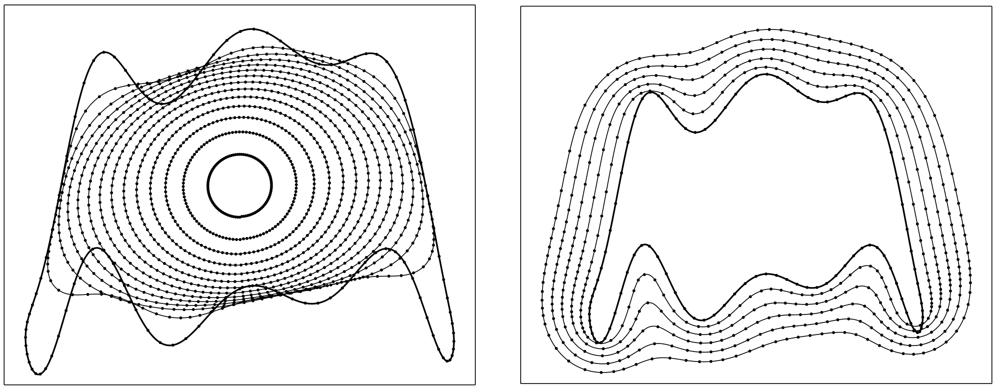

FIG. 6.7. *Isotropic curvature driven motion of an initial curve with high variations in curvature including uniform tangential redistribution of grid points;* $\beta(k,\nu) = \varepsilon k + F$, *with* $\varepsilon = 1$, $F = 0$ *(left) and* $\varepsilon = 1$, $F = -10$ *(right).*

Local lengths are updated by the formula:

$$r_i^j = \frac{r_i^{j-1} + \tau\omega M^{j-1}}{1 + \tau(B^{j-1} + \omega)}, \quad i = 1, ..., n, \quad r_0^j = r_n^j, \quad r_{n+1}^j = r_1^j. \tag{6.28}$$

The *tridiagonal system for discrete values of the curvature* reads as follows:

$$a_i^j k_{i-1}^j + b_i^j k_i^j + c_i^j k_{i+1}^j = d_i^j, \quad i = 1, ..., n, \quad k_0^j = k_n^j, \quad k_{n+1}^j = k_1^j, \tag{6.29}$$

where

$$a_i^j = \frac{\alpha_{i-1}^j}{2} - \frac{\delta(\tilde{x}_{i-1}^{j-1}, \nu_{i-1}^{j-1})}{q_{i-1}^j},$$

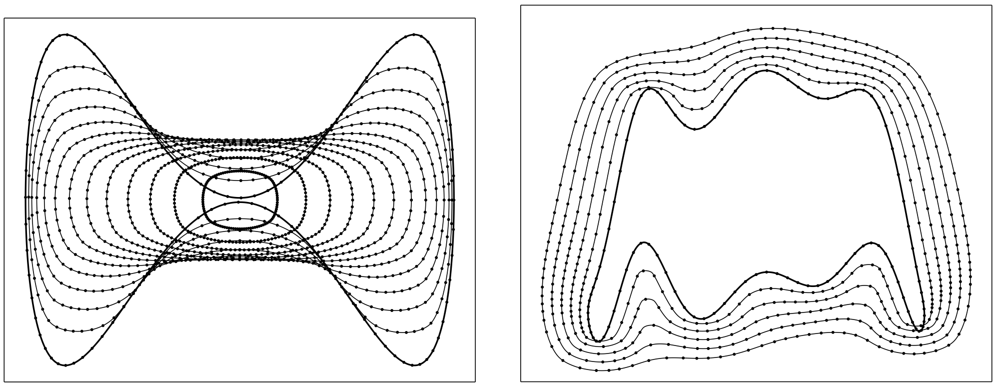

FIG. 6.8. *Anisotropic curvature driven motion of two initial curves including uniform tangential redistribution of grid points;* $\beta(k,\nu) = \gamma(\nu)k + F$*, with* $\gamma(\nu) = 1 - 0.6\cos(4(\nu - \frac{\pi}{4}))$*,* $F = 0$ *(left) and* $\gamma(\nu) = 1 - 0.7\cos(4(\nu - \frac{\pi}{4}))$*,* $F = -10$ *(right).*

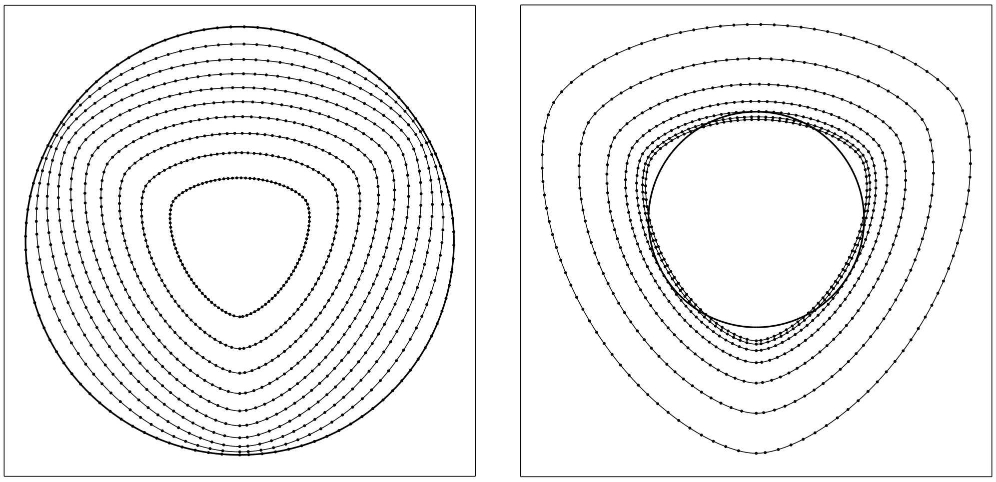

FIG. 6.9. *Anisotropic curvature driven motion of the initial unit circle including uniform tangential redistribution of grid points;* $\beta(k,\nu) = \gamma(\nu)k + F$*, with* $\gamma(\nu) = 1 - \frac{7}{9}\cos(3\nu)$*,* $F = 0$ *(left) and* $\gamma(\nu) = 1 - \frac{7}{9}\cos(3\nu)$*,* $F = -1$ *(right).*

$$
\begin{aligned}
b_i^j &= r_i^j\left(\frac{1}{\tau} - (B^{j-1} + \omega)\right) + \omega M^{j-1} - \frac{\alpha_i^j}{2} + \frac{\alpha_{i-1}^j}{2} + \frac{\delta(\tilde{x}_i^{j-1}, \nu_i^{j-1})}{q_{i-1}^j} + \frac{\delta(\tilde{x}_i^{j-1}, \nu_i^{j-1})}{q_i^j},\\
c_i^j &= -\frac{\alpha_i^j}{2} - \frac{\delta(\tilde{x}_{i+1}^{j-1}, \nu_{i+1}^{j-1})}{q_i^j},\\
d_i^j &= \frac{r_i^j}{\tau}k_i^{j-1} + \frac{c(\tilde{x}_{i+1}^{j-1}, \nu_{i+1}^{j-1}) - c(\tilde{x}_i^{j-1}, \nu_i^{j-1})}{q_i^j} - \frac{c(\tilde{x}_i^{j-1}, \nu_i^{j-1}) - c(\tilde{x}_{i-1}^{j-1}, \nu_{i-1}^{j-1})}{q_{i-1}^j}.
\end{aligned}
$$

The *tridiagonal system for new values of the tangent angle* is given by

$$A_i^j\nu_{i-1}^j + B_i^j\nu_i^j + C_i^j\nu_{i+1}^j = D_i^j,\ \ i = 1, ..., n,\ \ \nu_0^j = \nu_n^j,\ \ \nu_{n+1}^j = \nu_1^j, \tag{6.30}$$

where

$$A_i^j = \frac{\alpha_{i-1}^j + \beta'_\nu(x_{i-1}^{j-1}, \frac{1}{2}(k_i^j + k_{i-1}^j), \frac{1}{2}(\nu_i^{j-1} + \nu_{i-1}^{j-1}))}{2} - \frac{\delta(\tilde{x}_i^{j-1}, \nu_i^{j-1})}{q_{i-1}^j},$$

$$B_i^j = \frac{r_i^j}{\tau} - (A_i^j + C_i^j),$$

$$C_i^j = -\frac{\alpha_i^j + \beta'_\nu(x_i^{j-1}, \frac{1}{2}(k_i^j + k_{i+1}^j), \frac{1}{2}(\nu_i^{j-1} + \nu_{i+1}^{j-1}))}{2} - \frac{\delta(\tilde{x}_i^{j-1}, \nu_i^{j-1})}{q_i^j},$$

$$D_i^j = \frac{r_i^j}{\tau}\nu_i^{j-1} + \nabla_x \beta(\tilde{x}_i^{j-1}, \nu_i^{j-1}, k_i^j).(\cos(\nu_i^{j-1}), \sin(\nu_i^{j-1})).$$

To derive discretization of (6.25) we integrate it over the dual flowing control volume

$$\int_{\tilde{x}_i}^{\tilde{x}_{i+1}} \partial_t x ds = \int_{\tilde{x}_i}^{\tilde{x}_{i+1}} \delta(x,\nu)\partial_s^2 x ds + \int_{\tilde{x}_i}^{\tilde{x}_{i+1}} \alpha \partial_s x ds + \int_{\tilde{x}_i}^{\tilde{x}_{i+1}} \vec{c}(x,\nu) ds,$$

$$q_i \frac{dx_i}{dt} = [\delta(x,\nu)\partial_s x]_{\tilde{x}_i}^{\tilde{x}_{i+1}} + \int_{\tilde{x}_i}^{\tilde{x}_{i+1}} \partial_s \delta(x,\nu)\partial_s x ds + \alpha_i(\tilde{x}_{i+1} - \tilde{x}_i) + q_i \vec{c}(x_i, \frac{1}{2}(\nu_i + \nu_{i+1})),$$

$$q_i \frac{dx_i}{dt} = \delta(\tilde{x}_{i+1}, \nu_{i+1})\frac{x_{i+1} - x_i}{r_{i+1}} - \delta(\tilde{x}_i, \nu_i)\frac{x_i - x_{i-1}}{r_i} -$$

$$\frac{\delta(\tilde{x}_{i+1}, \nu_{i+1}) - \delta(\tilde{x}_i, \nu_i)}{q_i}(\tilde{x}_{i+1} - \tilde{x}_i) + \alpha_i(\tilde{x}_{i+1} - \tilde{x}_i) + q_i \vec{c}(x_i, \frac{1}{2}(\nu_i + \nu_{i+1})).$$

By replacing $\tilde{x}_i$ with the average of grid points, time derivative by time difference and using a semi-implicit approach in nonlinear terms we end up with *two tridiagonal systems for updating the position vector*

$$\mathcal{A}_i^j x_{i-1}^j + \mathcal{B}_i^j x_i^j + \mathcal{C}_i^j x_{i+1}^j = \mathcal{D}_i^j, \ \ i = 1, ..., n, \ \ x_0^j = x_n^j, \ \ x_{n+1}^j = x_1^j, \tag{6.31}$$

where

$$\mathcal{A}_i^j = -\frac{\delta(\tilde{x}_i^{j-1}, \nu_i^j)}{r_i^j} - \frac{\delta(\tilde{x}_{i+1}^{j-1}, \nu_{i+1}^j) - \delta(\tilde{x}_i^{j-1}, \nu_i^j)}{2q_i^j} + \frac{\alpha_i^j}{2},$$

$$\mathcal{B}_i^j = \frac{q_i^j}{\tau} - (\mathcal{A}_i^j + \mathcal{C}_i^j),$$

$$\mathcal{C}_i^j = -\frac{\delta(\tilde{x}_{i+1}^{j-1}, \nu_{i+1}^j)}{r_{i+1}^j} + \frac{\delta(\tilde{x}_{i+1}^{j-1}, \nu_{i+1}^j) - \delta(\tilde{x}_i^{j-1}, \nu_i^j)}{2q_i^j} - \frac{\alpha_i^j}{2},$$

$$\mathcal{D}_i^j = \frac{q_i^j}{\tau} x_i^{j-1} + q_i^j \vec{c}(x_i^{j-1}, \frac{1}{2}(\nu_i^j + \nu_{i+1}^j)).$$

The *initial quantities* for the algorithm are given by (6.16) – (6.18).

6.4. Computational results for a position dependent driving force. In this subsection we present results of computations with a general form of the normal velocity $v = \beta(x,k,\nu) = \delta(x,\nu)k + c(x,\nu)$ where effects of anisotropy, weighting of the curvature by a position function, constant forcing term and driving force in the form of a vector field projected to the normal are included. In our experiment shown in Figure 6.10 we chose

$$\delta(x,\nu) = x_1^2 + x_2^2, \ \ c(x,\nu) = (-x_1, -x_2).\vec{N} = x_1 \sin\nu - x_2 \cos\nu \tag{6.32}$$

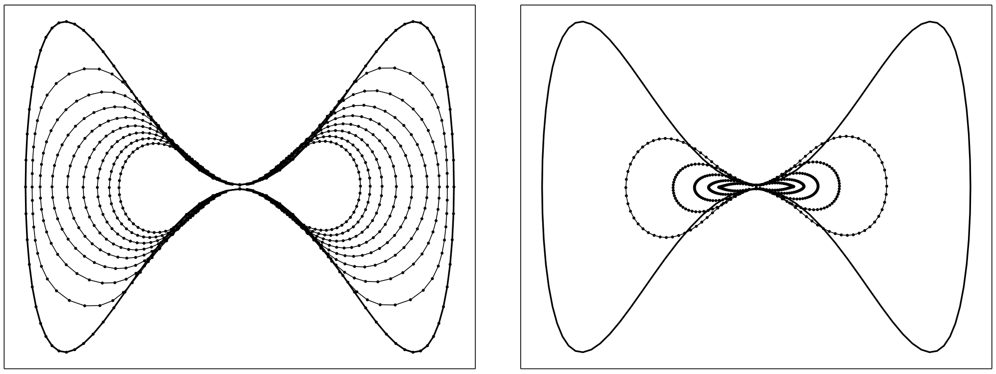

FIG. 6.10. *Curve evolution governed by* $v = (x_1^2 + x_2^2)\, k + (-x_1, -x_2).(-\sin\nu, \cos\nu)$.

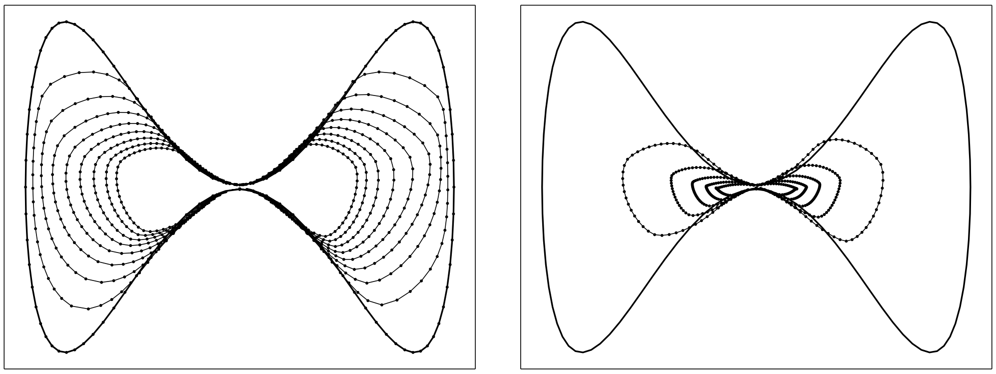

FIG. 6.11. *Curve evolution governed by* $v = (1 - \frac{8}{9}\cos(3\nu))(x_1^2 + x_2^2)\, k + (-x_1, -x_2).(-\sin\nu, \cos\nu)$.

and for Figure 6.11 we considered

$$\delta(x,\nu) = (1 - \frac{8}{9}\cos(3\nu))(x_1^2 + x_2^2), \;\; c(x,\nu) = x_1 \sin\nu - x_2\cos\nu\,. \tag{6.33}$$

In Figures 6.12-6.13 we considered the same regularizing function δ but c was modified by adding a constant driving force, e.g. $c(x,\nu) = x_1\sin\nu - x_2\cos\nu - 0.5$.

In all presented experiments we used 100 grid points representing a curve, time step $\tau = 0.001$ and redistribution parameters were chosen as: $\kappa_1 = \kappa_2 = 10$. In Figures 6.10-6.13 left we plotted an initial curve and then each $25th$ time step until the time $t = 0.2$. In the right parts of figures we continued visualization starting at time $t = 0.2$ and then plotting each $200th$ time step until the time $t = 1.0$ (in Figures 6.10-6.11) respectively until the time $t = 1.6$ (in Figures 6.12-6.13). In the first two cases we can see isotropic and anisotropic shrinking of curves leading to a blow-up of the isoperimetric ratio. In the last two figures we can see convergence to isotropic and anisotropic asymptotical shapes.

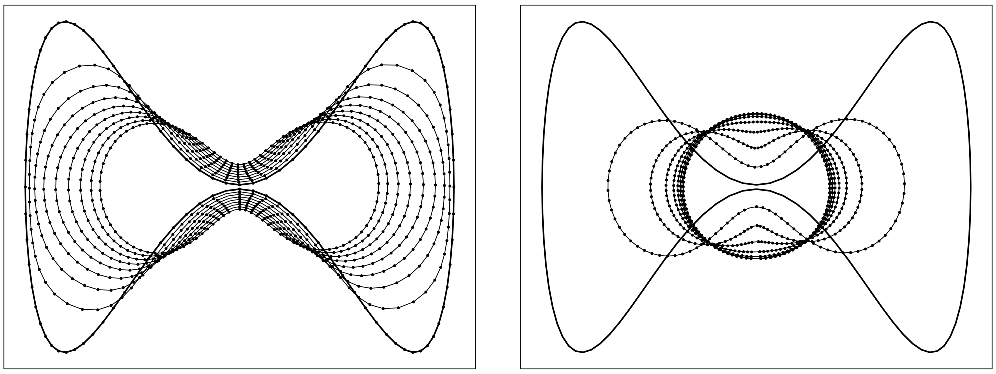

FIG. 6.12. *Curve evolution governed by* $v = (x_1^2 + x_2^2)\, k + (-x_1, -x_2).(-\sin\nu, \cos\nu) - 0.5$.

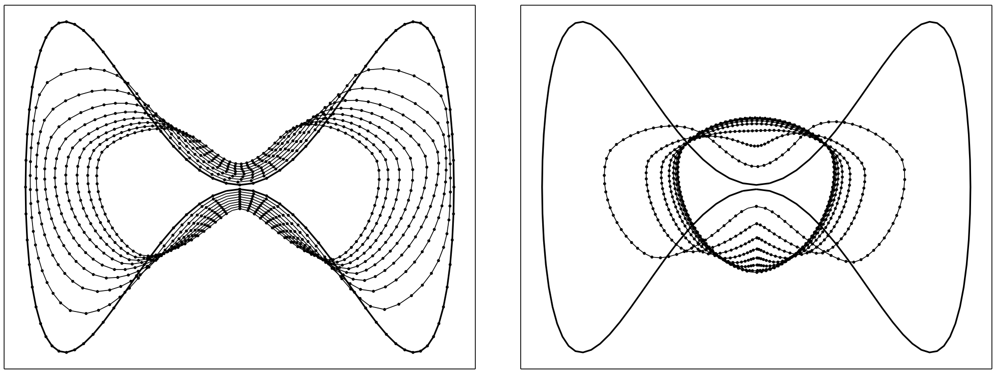

FIG. 6.13. *Curve evolution governed by* $v = (1 - \frac{8}{9}\cos(3\nu))(x_1^2 + x_2^2)\, k + (-x_1, -x_2).(-\sin\nu, \cos\nu) - 0.5$.

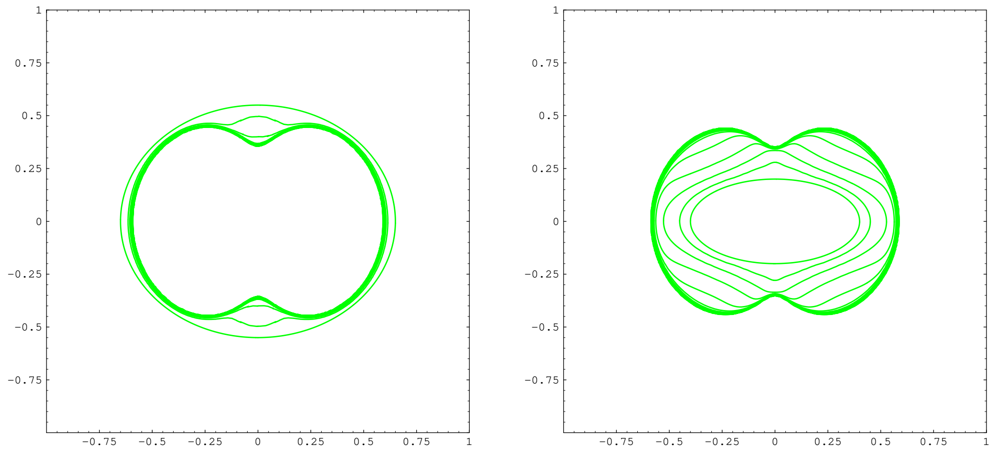

FIG. 6.14. *Convergence of an initial curve to the edge, from outside (left) and from inside (right).*

6.5. Image segmentation. Next we apply the computational method from subsection 6.3 to the image segmentation problem. Following the original motivation described in subsection 2.2 we consider $v = \varepsilon\phi(x)k - b(\phi(x))\nabla\phi(x).\vec{N}$, with $\phi(x) = h(|\nabla u_0(x)|)$, $h(s) = \frac{1}{1+s^2}$. As a first example, we considered an artificial image with the intensity function u_0 (see Figure 2.1 (left) and Figure 6.15 (right)) given by

$$u_0(x_1, x_2) = 0.5 + \frac{1}{10\pi}\text{arctg}\left(12.5 - \frac{100(x_1^2 + x_2^2)}{\left(1 + \frac{x_1^2}{1.5x_1^2 + 0.5x_2^2}\right)^2}\right). \tag{6.34}$$

We have inserted an initial curve (an ellipse) with resolution of 400 grid points inside the image. In the first experiment the initial curve belongs to the exterior of a Jordan curve representing the edge. In the second experiment it belongs in the interior of this Jordan curve and in the last experiment the initial ellipse crosses the edge. In all three cases we can see convergence of the initial curve to the curve representing the edge position. In all three experiments the limiting curves coincide up to a very high level of accuracy. The evolutions are plotted in Figure 6.14 and Figure 6.15 left, the final curve together with intensity image are given in Figure 6.15 right. In computations we have used the time step $\tau = 0.0001$, $\kappa_1 = \kappa_2 = 10$ and we evolved the initial curve until variations in the length and enclosed area are less than a prescribed tolerance (10^{-5}). Outer evolution stopped after 900 steps, inner ones after 2200 and those with initial curve crossing the edge stopped after 360 time steps. We considered $\varepsilon = 0.1$ and $b(\phi(x)) = \frac{0.5}{1-\phi(x)+\min_x \phi(x)}$. A function b was suitably chosen in order to achieve a faster evolution of the curve in "nearly flat" regions of the image.

The last numerical experiment is shown in Figures 6.16- 6.18. We follow an edge in a 2D slice of the real 3D echocardiography (filtered by the method of [37]) - see Figure 6.16. The testing data set is a courtesy of Prof. Claudio Lamberti, DEIS, University of Bologna, Italy. The initial ellipse is inserted into the slice close to an expected edge (Figure 6.17). Then it evolves using time step $\tau = 0.0001$, $\kappa_1 = 20$, $\kappa_2 = 1$ until the limiting curve is formed (400 time steps). This curve, representing the edge in the slice can be seen in Figure 6.18.

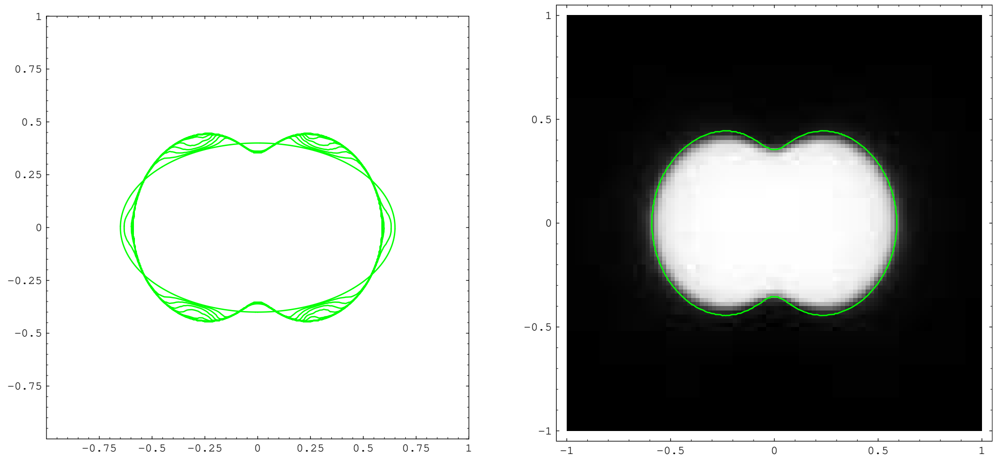

FIG. 6.15. *Convergence to the edge of an initial curve crossing the edge (left); the density plot of the image intensity function together with the limiting curve representing the edge position (right).*

REFERENCES

[1] U. ABRESCH, J. LANGER, *The normalized curve shortening flow and homothetic solutions,* J. Diff. Geom., 23 (1986), pp. 175–196.

[2] L. ALVAREZ, F. GUICHARD, P. L. LIONS, J. M. MOREL, *Axioms and Fundamental Equations of Image Processing,* Archive for Rat. Mech. Anal., 123 (1993), pp. 200–257.

[3] S. B. ANGENENT, *Parabolic equations for curves on surfaces I: Curves with p–integrable curvature,* Annals of Mathematics, 132 (1990), pp. 451–483.

[4] S. B. ANGENENT, *Parabolic equations for curves on surfaces II: Intersections, blow–up and generalized solutions,* Annals of Mathematics, 133 (1991), pp. 171–215.

[5] S. B. ANGENENT, *Nonlinear analytic semiflows,* Proc. R. Soc. Edinb., Sect. A, 115 (1990), pp. 91–107,

[6] S. B. ANGENENT, M. E. GURTIN, *Multiphase thermomechanics with an interfacial structure 2. Evolution of an isothermal interface,* Arch. Rat. Mech. Anal., 108 (1989), pp. 323–391.

[7] S. B. ANGENENT, M. E. GURTIN, *Anisotropic motion of a phase interface. Well–Posedness of the initial value problem and qualitative properties of the interface,* J. Reine Angew. Math., 446 (1994), pp. 1–47.

[8] S. B. ANGENENT, M. E. GURTIN, *General contact angle conditions with and without kinetics,* Quarterly of Appl. Math., 54, 3 (1996), pp. 557–569.

[9] M. BENEŠ. *Mathematical and computational aspects of solidification of pure crystallic materials,* Acta Math. Univ. Comenianae, 70 (2001), pp. 123–151.

[10] G. CAGINALP, *The dynamics of a conserved phase field system: Stefan-like, Hele-Shaw, and Cahn-Hilliard models as asymptotic limits,* IMA J. Appl. Math., 44 (1990), pp. 77–94.

[11] V. CASELLES, F. CATTÉ, T. COLL, F. DIBOS, *A geometric model for active contours in image processing,* Numerische Matematik, 66 (1993), pp. 1–31.

[12] V. CASELLES, R. KIMMEL, G. SAPIRO, *Geodesic active contours,* in: Proceedings International Conference on Computer Vision'95, Boston 1995, pp. 694–699.

[13] V. CASELLES, R. KIMMEL, G. SAPIRO, *Geodesic active contours,* International Journal of Computer Vision, 22 (1997), pp. 61–79.

[14] V. CASELLES, R. KIMMEL, G. SAPIRO, C. SBERT, *Minimal surfaces: a geometric three dimensional segmentation approach,* Numerische Matematik, 77 (1997), pp. 423–451.

[15] V. CATTÉ, P.L. LIONS, J.M.. MOREL, T. COLL, *Image selective smoothing and edge detection by nonlinear diffusion,* SIAM J. Numer. Anal., 29 (1992), pp. 182–193.

[16] K. DECKELNICK, *Weak solutions of the curve shortening flow,* Calc. Var. Partial Differ. Equ., 5 (1997), pp. 489–510.

[17] G. DZIUK, *Convergence of a semi discrete scheme for the curve shortening flow,* Mathematical Models and Methods in Applied Sciences, 4 (1994), pp. 589–606.

[18] G. DZIUK, *Discrete anisotropic curve shortening flow,* SIAM J. Numer. Anal., 36 (1999), pp. 1808–1830.

[19] M. GAGE, R. S. HAMILTON, *The heat equation shrinking convex plane curves,* J. Diff. Geom., 23 (1986),

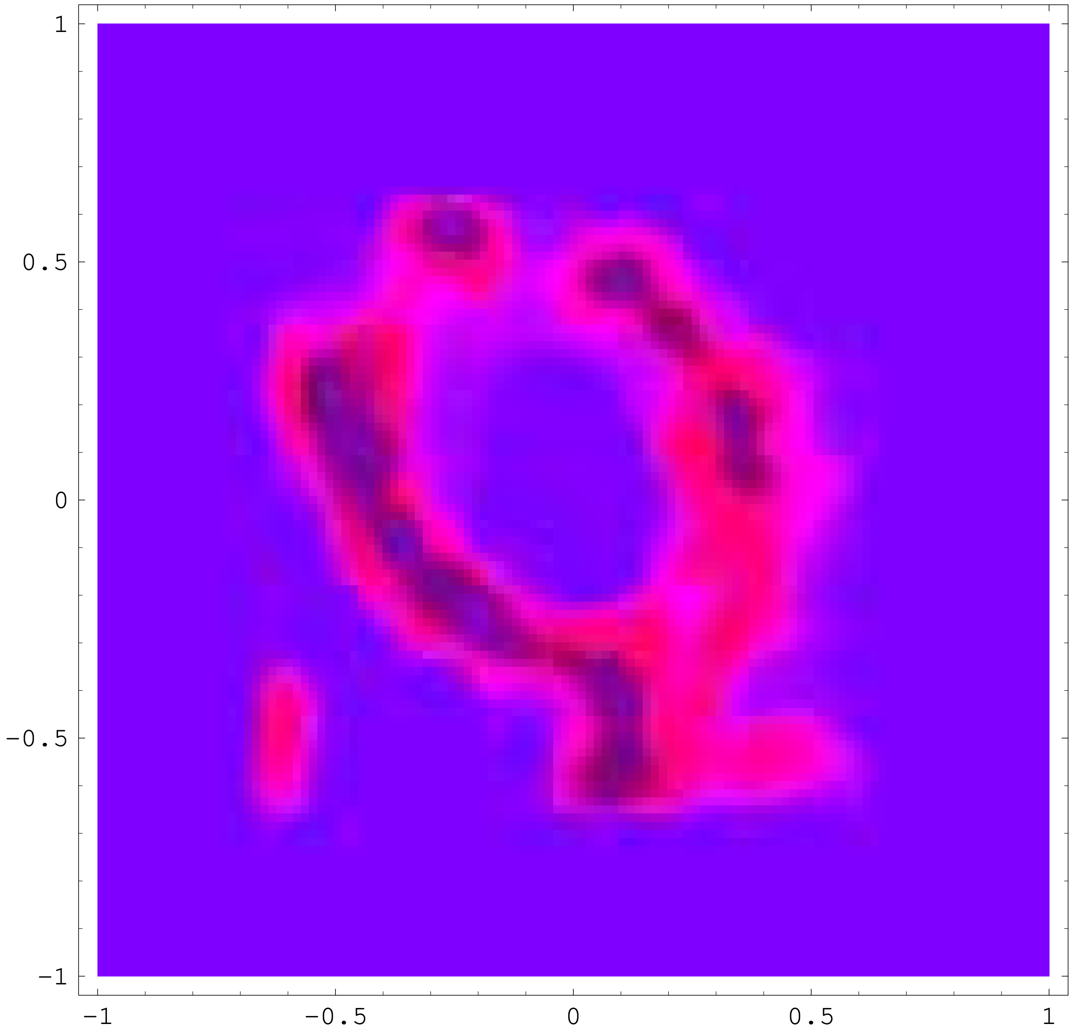

FIG. 6.16. *2D slice of a prefiltered 3D echocardiography.*

pp. 69–96.

[20] M. GRAYSON, *The heat equation shrinks embedded plane curves to round points,* J. Diff. Geom., 26 (1987), pp. 285–314.

[21] T.Y. HOU, J. LOWENGRUB, M. SHELLEY, *Removing the stiffness from interfacial flows and surface tension,* J. Comput. Phys., 114 (1994), pp. 312–338.

[22] T.Y. HOU, I. KLAPPER, H. SI, *Removing the stiffness of curvature in computing 3-d filaments,* J. Comput. Phys., 143 (1998), pp. 628–664.

[23] J. KAČUR, K. MIKULA, *Solution of nonlinear diffusion appearing in image smoothing and edge detection,* Applied Numerical Mathematics, 17 (1995), pp. 47–59.

[24] M. KASS, A. WITKIN, D. TERZOPULOS, *Snakes: active contour models,* International Journal of Computer Vision, 1 (1987), pp. 321–331.

[25] S. KICHENASSAMY, A. KUMAR, P. OLVER, A. TANNENBAUM, A. YEZZI, *Gradient flows and geometric active contours models,* in Proceedings International Conference on Computer Vision'95, Boston (1995)

[26] S. KICHENASSAMY, A. KUMAR, P. OLVER, A. TANNENBAUM, A. YEZZI, *Conformal curvature flows: from phase transitions to active vision* Arch. Rational Mech. Anal., 134 (1996), pp. 275–301.

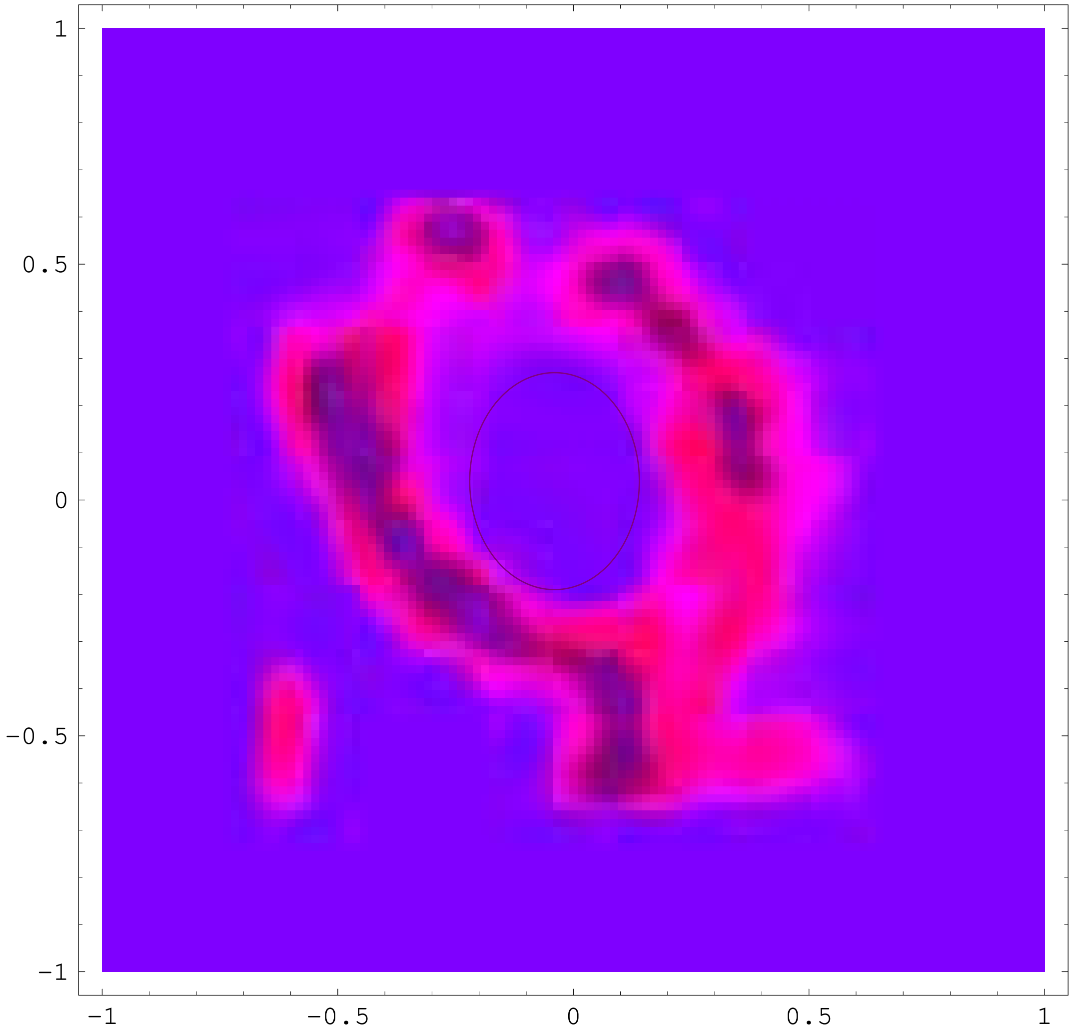

FIG. 6.17. *The initial ellipse is inserted into the slice.*

[27] M. KIMURA, *Numerical analysis for moving boundary problems using the boundary tracking method,* Japan J. Indust. Appl. Math., 14 (1997), pp. 373–398.

[28] R. MALLADI, J. SETHIAN, B. VEMURI, *Shape modeling with front propagation: a level set approach,* IEEE Trans. Pattern Analysis and Machine Intelligence, 17 (1995), pp. 158–174.

[29] K. MIKULA, J. KAČUR, *Evolution of convex plane curves describing anisotropic motions of phase interfaces,* SIAM J. Sci. Comput., 17 (1996), pp. 1302–1327.

[30] K. MIKULA, *Solution of nonlinear curvature driven evolution of plane convex curves,* Applied Numerical Mathematics, 21 (1997), pp. 1–14.

[31] K. MIKULA, D. ŠEVČOVIČ, *Solution of nonlinearly curvature driven evolution of plane curves,* Applied Numerical Mathematics, 31 (1999), pp. 191–207.

[32] K. MIKULA, D. ŠEVČOVIČ, *Evolution of plane curves driven by a nonlinear function of curvature and anisotropy,* SIAM J. Appl. Math., 61 (2001), pp. 1473–1501.

[33] S. OSHER, J. SETHIAN, *Fronts propagating with curvature dependent speed: algorithm based on Hamilton-Jacobi formulation,* J. Comput. Phys., 79 (1988), pp. 12–49.

[34] R. NOCHETTO, M. PAOLINI, C. VERDI, *Sharp error analysis for curvature dependent evolving fronts,* Math-

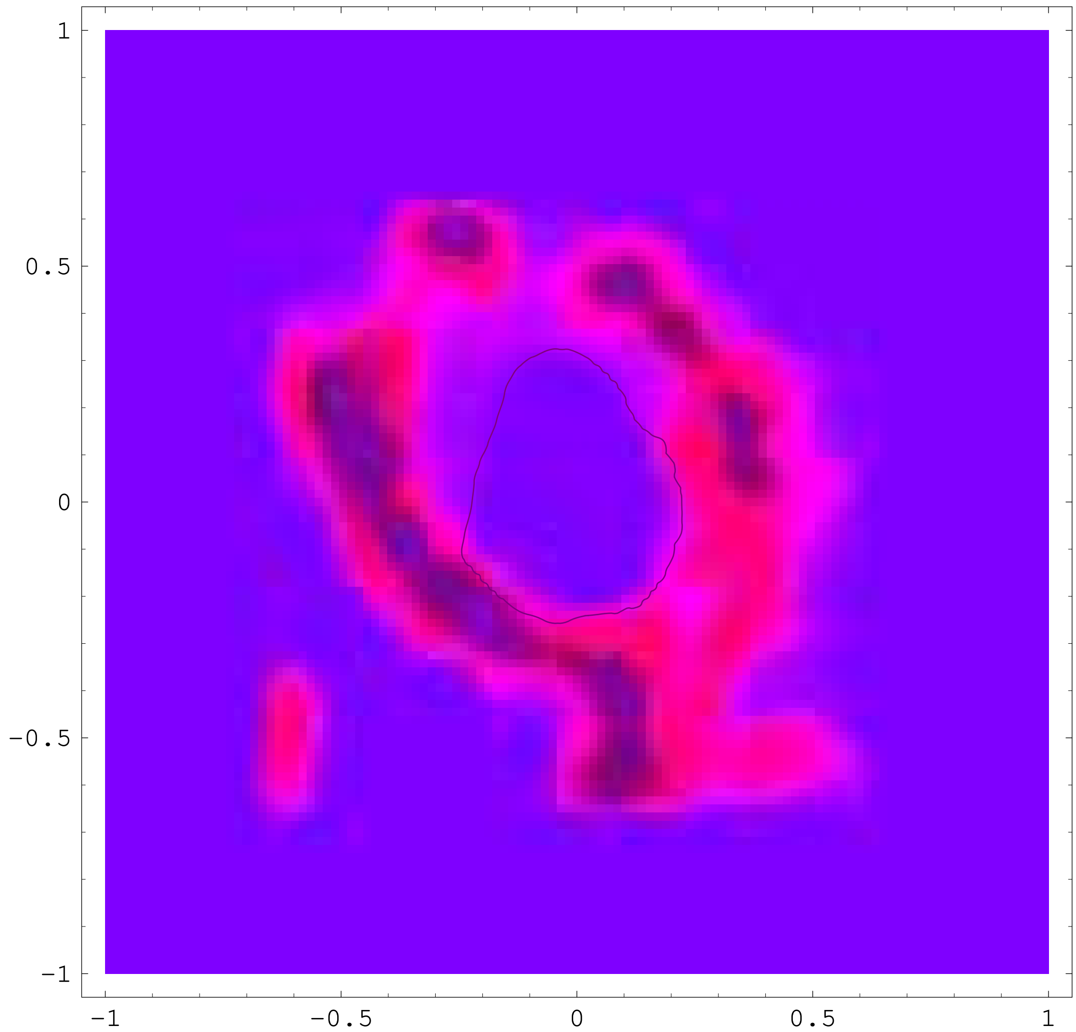

FIG. 6.18. *The slice together with the limiting curve representing the edge.*

ematical Models and Methods in Applied Sciences, 3 (1993), pp. 711–723.

[35] P. PERONA, J. MALIK, *Scale space and edge detection using anisotropic diffusion,* Proc. IEEE Computer Society Workshop on Computer Vision (1987)

[36] G. SAPIRO, A. TANNENBAUM, *On affine plane curve evolution,* J. Funct. Anal., 119 (1994), pp. 79–120.

[37] A. SARTI, K. MIKULA, F. SGALLARI, *Nonlinear multiscale analysis of three-dimensional echocardiographic sequences,* IEEE Trans. on Medical Imaging, 18 (1999), pp. 453–466.

[38] A. SCHMIDT, *Computation of three dimensional dendrites with finite elements,* J. Comput. Phys., 125 (1996), pp. 293–312.

[39] J.A. SETHIAN, *Level Set Methods and Fast Marching Methods: Evolving Interfaces in Computational Geometry, Fluid Mechanics, Computer Vision, and Material Science,* Cambridge University Press, New York, 1999.